

“Organic-Inorganic Hybrid Materials from Sonogels”

Nicolás de la Rosa-Fox^{*}, Manuel Piñero^a and Luis Esquivias.
Dpto. Física Materia Condensada. Facultad de Ciencias
^a Dpto. Física Aplicada. CASEM.
Universidad de Cádiz. 11510 Puerto Real (Cádiz). SPAIN.

Table of Contents.

- 1 – Introduction to sol-gel process.
- 2.- Sol-Gel Process steps (mixing, gelation, aging, drying and sintering)
- 3.- Sonogels
 - 3.1.- Pure silica sonogels (sonocatalysis, sonogel gelation)
 - 3.2.- OIHM (Ormosil, sono-ormosil)
 - 3.3.- Wet sonogels and hard sono-ormosil.
 - 3.4.- Dry Sonogels (Xerogels and Aerogels).
 - 3.5.- New trends in sono-ormosil
- 4.- Physical properties of OIHM.
 - 4.1.- Mechanical properties (ormosil, sono-ormosil)
 - 4.2.- Optical properties (ormosil, sono-ormosil)

^{*} To whom correspondence should be addressed (e-mail: nicolas.rosafox@uca.es)

Acronyms index.

BJH- Barret-Joyner-Halenda (PSD method)
BET- Brunauer-Emmet-Teller (specific surface area method)
CERAMER- CERAmic and polyMER
DCCA- Drying Control Chemical Additive
DMDES- Dimethyldiethoxysilane
DMS- Dimethyl siloxane
DSC- Differential Scanning Calorimetry
DTA- Differential Thermal Analysis
EtOH- Ethanol
HK- Horvath-Kawazoe (PSD method)
HPC- Hydroxypropyl cellulose
iPrOH- isopropanol
MAS NMR- Magic Angle Spinning NMR
MeOH- Methanol
MTES- Methyl-triethylsilane
MTMS- Methyl-trimethylsilane
NLO- Non-Linear Optics
NMR- Nuclear Magnetic Resonance (^1H , ^{29}Si , ^{13}C , ^{17}O for different isotopes)
OIHM- Organic-Inorganic Hybrid Materials
ORMOCER- ORganic MODified CERAmic
ORMOSIL- ORganic MODified SILicate
PDMS- Poly (dimethyl siloxane)
PDPS- Poly (diphenyl siloxane)
PEG- Poly(ethyleneglycol)
PEO- Poly(ethyleneoxide)
PMMA - Polymethylmetacrylate
PPO- Polyoxopropylene
PSD- Particle Size Distribution
PVA – Polyvinylalcohol
RCP – Random Close Packing
RDF- Radial Distribution Function

SAXS/SANS- Small-Angle X-ray/Neutron Scattering

SEM/TEM- Scanning/Transmission Electron Microscopy

TEOS- Tetraethyl ortosilicate

TGA- Thermogravimetric Analysis

TIPT- Tetraisopropyltitanate

TMOS- Tetramethyl ortosilicate

TMS- Tetramethylsilane

WAXS – Wide-Angle X-ray Scattering

XRD – X-Ray Difraccction

Some etymological terms¹

Aqueous -

Elastic -

Electric -

Hybrid - From Latin whose meant was "product of the cross of two different animals".

Hydro-philic -

Hydro-phobic -

Optic -

Oxygen – Formed from Greek oxys "acid" and gennao "I beget".

Permeable – From Latin "go through".

Plastic -

Polymer – From Latin Poly "many" and –mero "pure, without mixture".

Silica - From Latin silex "pebble".

¹ J. Corominas, in "Diccionario Etimológico de la Lengua Castellana" 3rd ed. (Gredos, Madrid, 1973)

1.-Introduction to Sol-Gel process

The sol-gel technique has been widely used in the preparation of transparent oxide glasses by hydrolysis and condensation of metal alkoxides since Ebelmen reported the first synthesis of silica from silicon alkoxide in 1844¹. In a strict sense, "sol-gel processing" is the synthesis of an oxide network via inorganic polymerization starting from molecular precursors in solution. This term frequently is extended to refer to the preparation of inorganic oxides by "wet chemistry". The sol-gel process provides as a new approach to the preparation of glasses and ceramics with many advantages over conventional methods. Pioneers^{2,3} claimed that this technique was particularly suitable for the synthesis of complicated multicomponent glasses because the liquid state favours homogeneous mixing at temperatures much lower than the fusion point.

In this way, Schroeder⁴ reported the preparation of vitreous layers of individual and mixed oxides (SiO_2 , TiO_2 and others) by hydrolysis and polycondensation of metal alkoxides. Also Mackenzie⁵ included the hydrolysis of metal alkoxides in his compilation of unconventional routes to glasses.

Until mid eighties, gel to glass conversion was considered the most interesting technological application for sol-gel processing and received most attention and effort. If asked about future trends in the sol-gel processing, not many scientists would have foreseen the research carried out at present in most sol-gel laboratories. The emphasis was on the chemical synthesis of materials at room temperature or slightly elevated temperatures and homogeneous multicomponent products of highly controlled purity. Since then, basic research resolved and explained the majority of the chemical and physical phenomena of sol-gel processing, and laid the foundations for a number of present and future applications. Currently, rheological properties of sols and gels are finding utility for preparing bulk product, films, membranes, fibers and composites^{6, 7, 8, 9, 10, 11}. Brinker and Scherer¹² in their excellent treatise on 'The Physics and Chemistry of Sol-Gel Processing' have exhaustively described the possibilities for sol-gel methods for synthesizing a large number of preforms.

Thus to begin understand this process, a gel can be considered, in the simplest picture, as a giant molecule, which has been formed as a consequence of the growth by condensation of polymers or aggregation of particles, but no latent heat is evolved. This giant molecule reaches across the vessel that contains it and the coherent solid 3-D network inside the fluid phase is known as a "gel". The solid phase particles range in size from 1 to 100 nm¹³. Gels are often classified either as *particulate* or *polymeric*^{14,15}. Particulate means that the solid phase forms by aggregation of dense, non-polymeric particles. Particulate gels are obtained by destabilization of an aqueous colloidal solution of oxides, hydroxides or mineral salts, also known as colloidal gel. While polymeric gel refers to an entangled network of quasilinear chains obtained by hydrolysis and polycondensation of metal alkoxides. The structure of this continuous solid network depends strongly by the replacement of the corresponding fluid phase. Like this, "*alcogel*" is termed when the pore liquor is alcohol and "*hydrogel*" when water is, at this step the structural changes process of the gel immersed in the liquid modify the reaction rates. When the liquid is removed we obtain an "*xerogel*", if slow evaporation of the pore liquid takes place or an "*aerogel*" if the pore liquid is removed in its hypercritical conditions of pressure and temperature.

When we move to the nineties, a new approach appears as the homogeneous combination of organic and inorganic precursors to form a hybrid structure. This offers a huge number of possibilities in the field of **organic-inorganic hybrid materials (OIHM)**^{16, 17, 18, 19, 20, 21, 22}.

Biocomposites are the best example of this OIHM produced by natural biomineralization²³. Bones, teeth, shells and in some leaves and stalks of plants are typical biocomposites in which an organic polymer matrix is reinforced by an inorganic deposit. As an example, amorphous silica is precipitated in the polysaccharide matrix of the rice plant, reinforcing it the leaves and stalks. Likewise the silica enhances photosynthesis due to the scattering effect and reduce water evaporation. In the animal kingdom, the mollusc shells are one typical example of hard organic-inorganic hybrid materials (OIHM). They consist in alternating layers of aragonite and organic matrix, giving one of the harder

natural composites. In this new field to mimicry the biomineralization process take the advantages of the organic polymers as flexibility, low density, toughness and formability whereas the inorganic part contributes with surface hardness, modulus strength, transparency and high refractive index²⁴

This route opens a wide possibility of material processing offered by the colloidal state. The low viscosity of sols allows the easy casting into a mold or the preparation of films. To a certain extent, these hybrid materials combine the advantages of the sol-gel process as metallo-organic precursors, organic solvents and low processing temperature, combined with the specific characteristics of the organic polymers as hydrophobic/hydrophilic parts, porosity control, electrochemical reactions. The combined of these bilateral actions act in the following way, inorganic part governs the properties of hardness, brittleness and transparency whereas density, porosity and thermal stability depend on the organic polymer²⁵. Such organic polymers can improve the physical and chemical properties, as an example can be mentioned the modification of the mechanical behaviour, easier processing of films and fibers, biochemical reactivity or modulation of the optical refractive index and NLO properties^{26, 27}. These hybrid networks can be divided into two main classes as a general classification, after Sanchez²⁸, whose aim is to control the length scale through soft chemistry (chimie douce):

Class I (network modifiers) in which the organic polymer or organic molecules are simply embedded into the inorganic matrix. No covalent bonds exist between both phases only weak interaction such as Van-der Waals forces, electrostatic or H bonds. As an example of this class I are the organic dyes or biomolecules incorporated in the porous inorganic gel. Via the H bond between organic and inorganic parts the transparency and no phase separation could be achieved.

Class II (network formers) in which the organic and inorganic parts establish covalent or ionic-covalent bonds. To this class correspond the hybrid materials that incorporate functionalised alkoxysilanes such as PDMS.

This sol-gel method is extensively used to obtain amorphous materials where the homogeneity is directly designed on a molecular scale, ranging from single-

phase to multi-phase systems. The combination of several precursors for the synthesis of nanostructured materials hybrid polymers are an open door in the chemical route and can be used to form nano-particles, coating, fibers or bulk solids with the corresponding technological applications.

On the other hand, in the ormosil picture based mainly in the silica as inorganic phase, we can distinguish three types after the classification of Mackenzie²²:

Type A-Entrapped organics: the organic molecule, such as a dye or pigment, can be mixed into the sol-gel solution. The resultant gel, casting as film or bulk should be useful and new optical, mechanical and chemical properties. From the pioneering work of Avnir et al.²⁹, which they encapsulated Rhodamine 6G in silica gel, numerous publications focused on silica as inorganic matrix, have been published. It is used as dye laser²⁹, photoconduction³⁰, second harmonics³¹, third order NLO³², chemical sensors³³, photochromics³⁴, etc. However, the low thermal stability of the organic molecules 200-300°C, for which the silica still remains extremely porous and would contain an important amount of OH groups and solvents, the inorganic gel matrix would continue to undergo structural transformations that affects to the mechanical and optical properties, this have some limits in the practical use of such hybrids materials.

Type B-Impregnated organics: In order to exploit the tuneable porosity of the silica gels, such as interconnecting pores, controllable size and size distribution, it is widely used as host for many materials including organics. The interaction between the organic polymer and the inorganic part is made via hydrogen bonds, which play an important role in avoiding phase separation and yielding transparent glass-like composites. S. Yano et al.³⁵ obtain hybrids with small amounts of silica that exhibit improved mechanical properties, mainly due to 1) nanometer-sized silica disperse evenly throughout the HPC (hydroxypropyl cellulose) polymer chains and 2) HPC chains strongly interact with silica or silanol through hydrogen bonding becoming entrapped between silica precipitates.

Other organic polymers such as PVA, PMMA, HPC, PEG, PEO, PPO, etc. Have been used via H bond between the organic and inorganic parts²⁸.

Type C-Chemically bonded organics-inorganics: In this case, the organic and inorganic are chemically bonded via covalent or ionic-covalent bonds. The stronger nature of the covalent bond improves much more the mechanical properties of the composites. One of the best systems to obtain OIHM by this approach is the combined reaction of silanol-terminated polymer as organic component with silicon alkoxide namely TEOS or TMOS as inorganic component. In the silanol-terminated polymers dominate the non-bridging oxygen Si-CH₃ groups depending on the average molecular weight. The end chain groups –OH or –OR radicals link the polymer with the silica network, via the termed "*copolymerisation*".

Type C ormosil between TEOS and PDMS can be promoted by high power ultrasounds termed "*sono-ormosil*" which are denser with enhanced mechanical properties. As a comparison in the Table 1 are shown the Vickers hardness of some representative materials in relation with the sono-ormosil.

Placing these materials between the softest glasses and the hardest transparent plastics. With higher PDMS content the ormosil behaves as a rubbery material, as we will see later.

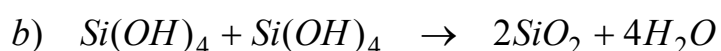
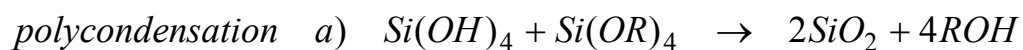
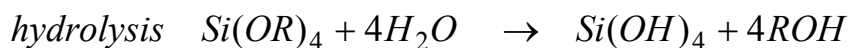
One proposed route to these materials, incorporates an organic phase in the inorganic precursor sol in combination with the assisted high power ultrasounds^{36,37,38}. Given that in sol-gel process little or no heating is required, organic molecules with low thermal stability can be incorporated into inorganic ceramic or glassy host. In this way, the "*sonogel*" route is another approach to sol-gel process modifications. The sound waves in the liquid promote the chemical reactions by means the cavitations phenomena. The gel obtained by this way, termed "*sonogel*", differs from classic gels in some parameters, they are denser with finer porosity, and then a homogeneous structure can be done. Ormosil can also be excellent matrices for non-linear optical materials due to the high transparency, inertness, mechanical strength and ease of preparation³⁹. In this way semiconductor quantum dots have been dispersed in ormosil⁴⁰ as well as dye laser is enhanced⁴¹.

2- Sol-gel process steps

(mixing, gelation, aging, drying and sintering).

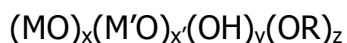
Several steps are involved in the sol-gel process in order to obtain a gel, namely: mixing, gelation, aging, drying and sintering. At each step there are many interesting physical and chemical factors that convert these areas in a fascinating subject each.

MIXING- it is commonly asserted that the more attractive feature of sol-gel processing is the possibility of tailoring unique materials, especially, by polymerization of a metalorganic compound to a polymeric gel. The key is to design the proper monomer that will polymerise to form M-O-M structures. Metal alkoxides, $M(OR)_n$, fulfils these requirements, where M is the metal and R an alkyl radical. Popular choices used in the preparation of silica-based gels are tetramethoxysilane, $Si(OCH_3)_4$, and tetraethoxysilane, $Si(OC_2H_5)_4$, known as TMOS and TEOS, respectively. The liquid alkoxide precursor $Si(OR)_4$ reacts with water and undergo hydrolysis and polycondensation reactions under the following schema, in presence of a common solvent (normally alcohol):



which are produced simultaneously and generally incomplete, but the attainable final oxide is accomplished. The final result of the above reactions is a colloidal dispersion of extremely small particles (1-2 nm) that finally form a 3-D entangled network of the corresponding inorganic oxide. Hydrolysis and polycondensation can be accelerated or slowed down by employing appropriate acid or base catalyst. Depending on the amount of water present, hydrolysis may go to completion or stop while the metal is only partially hydrolysed. In the case where several different cations are used to form mixed-oxide networks, a complexation step may be required initially. When the alkoxide precursors have

different hydrolysis rates (e.g. Al or Ti with regard to Si), a prehydrolysis of the alkoxysilane is preferred^{6,12}. After a complex sequence of polymerization, sol formation and gelation, a high surface area microporous gel constituted of small particles (≈ 2 nm), with a formula approximated by:



is formed. Radicals -OH and -OR account for reaction by-products that can reasonably easily leave the system yielding a complex three-dimensional oxide polymer -M-O-M'-O-M- which preconfigures the network of corresponding oxide glasses.

GELATION- with the time the polycondensation of silicon alkoxide produce colloidal particles that link together to become a 3-D network. In this process the catalyst play an important role due to the ionic charge of the silica particles, with a direct influence on the polycondensation rate. Thus, at low pH for example, the silica particles bear very little ionic charge and thus can collide and aggregate into chains forming a polymeric gel, in other length scale this gel should be similar to a spaghetti dish. This effect is produced around the silica isoelectric point at pH=1.7 where the surface charge is zero. On the opposite side, at high pH, where the rate of dissolution is higher, the particles grow in average size and diminish in number as the smaller ones dissolve (positive curvature) and the silica is deposited upon the larger ones⁴², in such a case is formed a colloidal gel, as a visual picture this gel should be similar to a bean pot. As a direct consequence of the visual pictures outlined a lower density will be observed in the colloidal gels.

The drastic change in the rheological behaviour of the sol is used to identify the gel point. In this way Saks and Sheu⁴³ use a precise method to measure the gelation time. They measured the complex shear modulus that consist in a viscous contribution (loss modulus G'') and an elastic contribution (storage modulus G'), then the loss tangent ($\tan \delta = G''/G'$) gives the behaviour in the gel point by a maximum followed by an abrupt decrease. Using ²⁹Si NMR Vega and Scherer⁴⁴ conclude that the structure at the gel point is highly variable, influencing factors such as dilution, pH and temperature, which give rise to

many observed trends as extent of branching, colloidal versus polymeric, fractal versus homogeneous size distribution.

From the classical theory of polymerization developed by Flory⁴⁵ to the modern fractal geometry⁴⁶ and the percolation theory⁴⁷, all of them treat to explain this critical transition. Flory theory result incomplete because no rings are permitted and as a consequence the mass of the cluster (Bethe lattice or Cayley tree) increase as the fourth power of the size that is unrealistic⁴⁸. Percolation allows for rings or closed loops to form and so does not predict a divergent density for the cluster. The validity of the percolation theory is its power to predict the behaviour of some physical properties near the gel point^{12, 47, 49} (elastic modulus, viscosity, mean cluster size, cluster size distribution, gel volume fraction, etc.) by means the scaling laws and critical exponents. Fractal geometry is based on the cluster structure invariant with scale (a portion is structurally similar to the whole) and show a decrease of density with cluster size. Fractal objects are characterised by their fractal dimension D that may be defined by the relations for mass and surface fractals:

$$M \propto R^{D_m} \quad S \propto R^{D_s}$$

where M and S are the mass and the specific surface of the object and R is its average size. Mass and surface fractals never can be found in the same length scale. D_m takes values, never integer that correspond to the Euclidean dimension, between 1 to 3, that is from a linear long polymer $D_m=1-1.5$ to branched and dendritic ones $D_m=1.5-2.5$, up to denser clusters $D_m \approx 3$. D_s values, on the other hand, increase from $D_s \approx 2$ for a smooth surface to $D_s \approx 3$ for a very rough one.

AGING- With time after gelation the solid network immersed in the pore liquor continues to evolve. This aging process occurs via three steps, polymerisation, syneresis and coarsening. Polymerization of unreacted hydroxyl groups increase the connectivity of the gel network, this process run parallel with some shrinkage. Syneresis is the spontaneous and irreversible shrinkage of the gel network resulting in expulsion of pore liquid, the driving forces of the flow liquid produce compressive stresses that draw the solid network into the liquid. Since

the fluid flow through porous media obeys Darcy's law⁵⁰, which states that the flux J is proportional to the gradient of the liquid pressure ∇P_L

$$J = -\frac{D}{\eta_L} \nabla P_L$$

where η_L is the viscosity of the liquid and D its permeability.

This process depends strongly on the catalyst being minimum at the isoelectric point (pH=1.7 for silica) where the particles are uncharged. Coarsening or ripening refers to a process of dissolution and reprecipitation driven by differences in solubility between surfaces with different radii of curvature⁴². This process not produce shrinkage of the network but influence the strengthening of the gel and depends by factors that affect the solubility, such as temperature, pH, concentration and type of solvents⁵¹.

DRYING- one of the main problems in the preparation of bulk materials is avoiding cracking of the gel during drying, due to the stresses caused by the capillary forces associated with the gas-liquid interfaces. Fractures are initiated if these stress differences are greater than the tensile strength of the material. According to Laplace's formula that stands for a capillary of radius r and a liquid having a wetting angle θ , the capillary pressure Δp is:

$$\Delta p = \frac{2\gamma \cos\theta}{r} \quad (1)$$

The pressure is proportional to the specific surface energy γ at the liquid-air interface. Considerable stresses can be generated in this way, for example for a pore radius of 2 nm filled with water ($\gamma=0.073 \text{ N m}^{-1}$) and assuming a perfect wetting, $\Delta P=73 \text{ MPa}$ ⁵². All actions on these parameters that tend to minimize the capillary pressure gradient and increase the mechanical strength of the network should enhance the probability of monolithic gel formation. The direct solution is to let the liquid evaporate at a very low rate. This strategy, although effective, is not practicable because of the long drying times required. It would take weeks, even months, to form a monolithic dried gel (xerogel). One alternative to accelerate drying is to add drying control chemical additives (DCCA) that modify the surface tension of the interstitial liquids, allowing fast elimination of the unwanted residues. DCCAs are incorporated in the starting

mixture before gelling and after an adequate heat-treatment, a crack-free xerogel results⁵³. Formamide is one of the most common DCCAs used for drying silica gels. The action of the formamide in the gelling process starts in the liquid state by inducing, under acidic catalysed conditions, a progressive increase of the solution pH with time. The mechanism that eliminates cracking is not yet well understood, although a few explanations are plausible. The hydrolysis reaction is generally faster and more complete under acidic conditions and the average condensation rate is maximized near pH=4. Consequently, formamide addition to acid-catalysed systems should allow efficient hydrolysis followed by a rapid condensation when formamide hydrolysis provokes an increase of the solution pH. Therefore, one effect of formamide addition may be gel strengthening. Small angle X-ray scattering (SAXS) was used to investigate the differences in structure and kinetics during aggregation of solutions with formamide. This technique measures the angular dependence of the intensity scattered by a sample with heterogeneous electron density. Monomer aggregation leads to clusters that can be described as statistical polymeric balls⁵⁴. The texture of the solution at the gel transition becomes finer as formamide content increases. The xerogel structure has been depicted as a hierarchy of several levels by means of models built up using the Monte-Carlo calculations, on the basis of random close packing (RCP) premises^{55, 56, 57, 58}. The effect of formamide addition is a decrease in the average cluster size at the gel transition suggesting that this additive enhances the nucleation of growing aggregates. These effects are consistent with observations that formamide increases the microhardness of wet gels and correspondingly the pore sizes of dried gels, while maintaining a narrow pore size distribution⁵⁹. On the other hand, the high viscosity of formamide leads to formation of a formamide layer on the gel surface. This would be likely reduces the capillary pressure in two ways: (1) by forming a surface film, it reduces the contact angle; (2) because of its low vapour pressure it evaporate very slowly, providing a plasticizing effect that minimizes crack formation.

Either way, the most efficient way of neutralizing the undesired effects of surface tension is to suppress the liquid-vapour interface. This is achieved by

treating the gel in an autoclave under supercritical conditions for the solvent, taking care that the path of the thermal treatment does not cross the equilibrium curve. This technique, initially developed by Kistler⁶⁰, was applied by Nicolaon and Teichner⁶¹ to gels obtained from metallorganic compounds. A systematic investigation design to optimise supercritical extraction conditions to produce monolithic aerogels was carried out at Montpellier^{62, 63, 64, 65}. Two different strategies can be used to bypass the critical point: (1) Adding an extra volume of liquid in the autoclave and the heating; (2) applying pressure using an inert gas before heating⁶⁶. The resulting product is a gel with its pores filled with air; the source of term *aerogel*. Aerogels are very porous and brittle materials. They are interesting products by themselves because of their very particular structure that, in some cases, can be described in terms of fractal geometry. A series of proceedings has been published devoted exclusively to these very unusual materials⁶⁷. They are extremely light, with densities as low as $0.01 \text{ g}\cdot\text{cm}^{-3}$, fulfilling the autosimilarity condition over one order of magnitude⁶⁸. Aerogels are one of the rare, true examples of fractal materials. Fricke has investigated and reviewed aerogels as engineering materials^{69,70,71}.

SINTERING- this is the process of the network densification, which is driven by interfacial energy. Solid network moves by viscous flow or diffusion to eliminate porosity. In gels with high pore surface areas the driving forces is great enough to produce sintering at exceptionally low temperatures, where the transport processes are relatively slow. Indeed, the kinetics of densification in gels are not simple because of the concurrent processes of dehydroxylation and structural relaxation. As an example, constant heating rate was used by Prassas et al.⁷² to study the sintering process in aerogels (70-90% porosity, $0.1\text{-}0.5 \text{ g}\cdot\text{cm}^{-3}$ density) and they conclude that several mechanism are involved in such sintering process. Below 700°C sintering is conducted by a diffusional process due to chemical reactions, while above 750°C begins the viscous flow mechanism and the activation energy of this process is related to the hydroxyl content.

Even though, the scope of the OIHM is not the obtaining dense glass due to the decomposition temperature of the organics, 200-300°C. However, some scientists have shown the persistence of Si-C bonds in the gels fired at 900°C⁷³. This fact is expected to enhance the mechanical and thermal properties produced by the pyrolysis process under inert atmosphere above 600°C turning the OIHM to a "black glass"⁷⁴.

3.- SONOGELS.

As it is described in the above paragraph, the alkoxide+water mixture needs a common solvent to react. Therefore, by subjecting that mixture to the action of high power ultrasounds it is possible to promote the hydrolysis and self-condensation of the alkoxide^{75, 38}. These reactions are produced in the small bubbles provoked by the cavitation phenomena. In this way, acoustic cavitation takes place inside the bubbles dispersed in whole liquid, the rapid compression/decompression of the sonic wave (20 kHz) causes the bubble radius to oscillate around some equilibrium size and finally collapse. When high power ultrasounds are used (~100 W output power) it is formed extremely hot-spots in the liquid following three discrete stages: nucleation, growth and implosive collapse^{76,77}. The harsh conditions generated on bubble collapse lead to the production of excited states to bond breakage and formation of free radicals. Thus, three areas of a cavitation system can be identified: The centre of the hot-spot is where the primary chemistry involved in, atomic and radical recombination takes place⁷⁸. The surrounding heterogeneous liquid is relatively unaffected, although species generated inside the bubble may diffuse out and react with reagents in the liquid. At this point, the interfacial region has very large gradients of temperature, pressure, surface tension, electrical field and rapid motion of molecules leading to a efficient mixing^{79,80}. It is interesting to note that the presence of foreign particles enhance the cavitation because of they act as nucleation sites.

The temperature inside the hot-spot has been estimated to be about several thousand Kelvin from the relationship⁸¹:

$$T_s = \frac{R \cdot P_s}{c_p \cdot P_x} T_0$$

where T_0 is the experimental reaction temperature, P_s the pressure of the liquid when bubble collapse, P_x the pressure of gas inside the bubble, R and c_p are the gas constant and the heat capacity of the bubble, respectively. Although the concept of cavitation hot-spot temperature must be considered here with care, it is possible to study the polymerisation rate by Arrhenius behaviour as:

$$k = A \exp\left(-\frac{E}{RT_s}\right)$$

where E is the apparent activation energy and A is constant. In this way, a high local temperature would give a very fast reaction rate.

The alkoxide-water mixture involved in this work can be classified, under the Luche's rule⁷⁹, as a heterogeneous system (liquid/liquid), in which ionic reactions are stimulated by mechanical effects, therefore the product of the reaction will be the same as in the absence of ultrasounds (classic or conventional method). Application of ultrasounds (sonochemistry) for the synthesis of organosilane and organosiloxane precursors has been studied by P. Boudjouk⁸² and J. Price⁸³.

3.1.- Pure Silica Sonogels.

This paragraph is focused to explain the systematic studies carried out on silicon alkoxide+water mixtures. The aim of such work was to elucidate the differences between the sonogels and the obtained by the conventional method, termed as classic.

Tarasevich reported the first observation of the TEOS/water mixture reaction under the action of high power ultrasounds in 1984⁸⁴. He described that reaction show an intense increase of the temperature with release of alcoholic vapours. He obtained a homogeneous and transparent solution in a few minutes. Afterwards, the Zarzycki's group in France began intensive work to establish the consequence of ultrasonic influence on the textural characteristics of the termed "sonogels"^{85,86,87}. Following in the same way, the Esquivias' group in Spain used the sonogel as matrices to encapsulated semiconductor

nanocrystals^{88,89}, organic dyes^{90,91} and hybrids organic-inorganic based on ORMOSIL^{40,92,93}. In recent years, the Mackenzie's group in USA applied the ultrasonic method to synthesised hybrid organic-inorganic based on PDMS and TEOS mixtures^{36, 37}.

SONOCATALYSIS-

The basic procedure in the laboratory follow the next steps.

1st- The corresponding mixture of the silicon alkoxide (TEOS or TMOS) and acidified water (pH<1) is placed into a double volume beaker. No reaction has been observed when was used neutral or basic water. It is possible to discern in the beaker a two-phase system, the water in the bottom and the alkoxide at the top, as can be seen in Fig. **1** schematically. At this point the tip of the ultrasonic device is placed immersed some millimetre into the liquid. Then the ultrasonic waves (20 kHz) are produced by an electrostrictive device equipped with an inox horn terminated in a titanium tip. The different ultrasonic horn type apparatus used by the above cited groups are shown in the following Table **2**.

2nd- During isonation the temperature increase abruptly to 80°C then stabilized at 70°C, the liquid blows-up indicating hydrolysis reaction break out. Since the boiling point of TEOS is 165°C, for the water is 100°C and the decomposition temperature of PDMS is about 250°C. The measured 70°C should be attributed to the boiling point of the ethanol release accounting for the exothermic hydrolysis reaction, this behaviour is illustrated in Fig. **2**. The produced alcohol promotes the polycondensation reaction becoming the gelation process. In some cases the vessel is surrounded by a thermostatic bath to ensure local temperature control.

3rd- how much ultrasonic energy is supplied to the solution?

It can be estimated by the temperature rise of a fixed volume (V) of water during the isonation and consequently calculated by the relationship:

$$W = \frac{dQ}{dt} = m_w c_w \frac{dT}{dt}$$

where dT/dt is the raising slope in the experimental curve of Fig. **2**. The mass of water and its specific heat are m_w and c_w , respectively.

Then the energy delivered by the ultrasounds will be:

$$U_s = \frac{W \cdot t}{V} \approx K \cdot t \left(J \cdot cm^{-3} \right)$$

where t is the insonation time in minutes. Some experimental K values are shown in the following Table **3**.

Many factors can affect these K values such as room temperature, catalyst, molar ratios water/TEOS, solvent/TEOS, beaker diameter and volume, sonic tip immersion in the liquid solution and its diameter.

4th- how much insonation time can be delivered to the solution?

There is an energy dose threshold when the liquid blows-up and a homogeneous solution is observed. In the other side, there is an energy dose for which the liquid gels in-situ, i.e. take place the gelation in the beaker during insonation. A transparent soft solid gel with the tip hole on top can be observed. Between these two limits in energy dose, one can be tuned in all range, in this way as a reference these energy dose $U_s(\text{min})$ and $U_s(\text{max})$ are shown in the following Table **4** for different reagents and contents, always in acidic water medium.

If the minimum dose is related with the hydrolysis reaction as can be seen in the Table **4**, the expected decrease of the hydrolysis rate due to the dilution is compensated by the action of ultrasounds. In the other limit, maximum dose related with the reticulation degree of the polycondensation rate accounts for a bigger reactivity of the TMOS as precursor. This effect is lowered by the presence of the PDMS organic polymer. This fact is a consequence of the different functionality of the involved molecules, $f=4$ for TEOS and TMOS and $f=2$ for PDMS.

5th- Once the sol is submitted to the decided ultrasonic energy dose, the liquid sol is kept in a hermetic container and let to gelled at the corresponding temperature. Since the sol is a low-viscosity liquid, it can be cast into a mould with a selected shape. In all cases was obtained a homogeneous and transparent solution. When the U_s applied is near $U_s(\text{max})$ the gelation takes

place in a few seconds, whereas in other cases this process takes several minutes or hours, depending on the ultrasonic energy dose.

GELATION OF SONOGELS-

When the sol passes from a viscous fluid to an elastic solid is taken as the gelation point. The gelation time is then taken as the time interval between the end of isonation and the above mentioned transition. This transition is visually estimated when the solution is no longer horizontal by tilting the container.

Fig. **3** shows the results of t_G vs. U_s for $H_2O/TEOS=4$ mixtures at several temperatures as a function of the ultrasonic energy dose (U_s). As a matter of fact, the temperature activates the gelation process as well as the increase of the ultrasonic energy dose. As can be observed two regimes are present separated by a level of $U_s=600 J cm^{-3}$. This point indicates the rapid increase in the polycondensation rate. As a reference for classic gels the gelation time takes of the order of several days for similar compositions.

From the Fig. **3** it is possible to establish the thermal behaviour of the gelation process. The plot of the t_G vs. $1/T$ is depicted on Fig. **4** for different ultrasonic energy doses. Considering an Arrhenius behaviour the corresponding linear fit give the activation energy of 50-70 kJ/mol-TEOS, that is somewhat of the same order of magnitude than those reported by Tiller et al.⁹⁴ of 45 kJ mol⁻¹-TEOS. Even though the pH dependence of the activation energy, the obtained activation energy for sonogels agrees with those reported by Coudurier et al.⁹⁵, for the condensation process of 61 kJ mol⁻¹ and for the aggregation one of 63 kJ mol⁻¹. This inform that the polycondensation in pure sonogels is well accomplished in the early stages, producing a more reticulated structure better than those in classic ones.

Fig. **5** shows the results of t_G for 90wt% TEOS-10wt%PDMS and molar ratio $H_2O/TEOS=2$, in which can also be observed the two regimes, but in this case of hybrid materials are separated by a level of $U_s=450 J cm^{-3}$, accounting for the influence of the PDMS organic polymer. This effect can be due to the chain breakage as a consequence of the ultrasounds influence, preventing also the

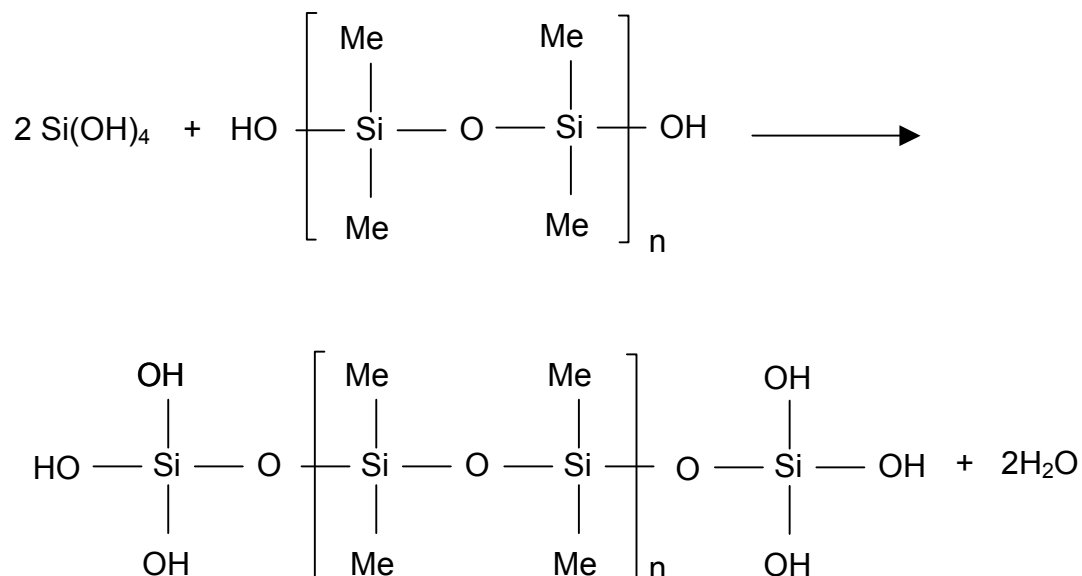
formation of rings. As a matter of fact, taking into account the slopes values from Figs **3** and **5** in the two linear regimes, in the first regime pure sonogels are two times faster and in the second one are three times. Dilution and average molecular weight of the PDMS polymer influence drastically this behaviour. Since the reactions in PDMS/TEOS hybrid system are more complicated than those in pure silicon alkoxides the activation energy is difficult to calculated.

3.2- ORGANIC-INORGANIC HYBRID MATERIALS (OIHM).-

ORMOSIL- Silica gel from alkoxides consist in an entangled of Si-O bonds to form a random porous network. This gel fracture because of their brittle nature. But the introduction in such network of polymers based on Si-C bonds, the gel becomes less rigid giving a softer network. Thus large monolithic pieces can be obtained without fracture.

In 1986, Wilkes et al.^{17,18} prepared successfully a new type of OIHM from the reaction of TEOS and silanol-terminated PDMS termed "ceramers". At the same time Schmidt¹⁹ proposed a new type of non-crystalline solid between organic and inorganic material, which he termed "ormosil". Subsequently other oxides such as ZrO₂, TiO₂ were also bonded to organic groups, which were termed "ormocer".

Ormosil can be excellent matrices because of their high optical transparency, inertness, mechanical strength and ease of preparation²². The combination of PDMS and hydrolysis products of TEOS present some similarities, which make the organic and inorganic components highly compatible. The copolymerisation of both precursors can be described schematically as:



The structure of the hybrid network strongly depends on catalysts, temperature and molar ratios of precursors. It is well known the hydrolysis-polycondensation behaviour of TEOS in acid catalyst giving polymeric structures that are less branched and fewer compacts than those obtained with basic catalyst. HCl catalysed PDMS-TEOS elastomers, the flexibility, gelation point and elongation at break are increased with the acid content as can be seen in the Table 5.

As can be stated from the above values, the ormosil samples could be rubbery, it is for that were termed "rubbery ormosil" by Mackenzie⁹⁶ and it is shown in the following Table 6.

This rubbery behaviour can understand by the fact that CH₃-Si-CH₃ non-bridging groups in the PDMS chain can rotate around the Si-O-Si bridge and the effective length of the linear PDMS chain can be decreased by coiling (around 50%). When an external stress is applied to the ormosil sample coiling of the PDMS chains will displace the silica units into the pores if the elasticity modulus is enough low. This process depends of the availability of pores, their size relative to the silica units, the average polymer length and its degree of linearity.

The reaction can be follow by ²⁹Si NMR spectroscopy as a function of time. As can be seen in the Fig. 6 the peak due to the Si atoms in the copolymer between TEOS and PDMS (D(Q) at δ= -17.5 ppm chemical shift) and the peak

due to the Si atoms polymerised from TEOS (Q^4 at $\delta = -109$ ppm) increase as the reaction time, whereas the signal of the Si atoms in hydroxyl terminated PDMS end groups and the corresponding to the monomers of TEOS (Q^0 at $\delta = -81$ ppm) decrease. The copolymerisation reaction is acid content dependent, higher acid content more hybrid reticulation is.

In the terminology of ^{29}Si NMR, Q^n represents a silicon atom bonded through oxygen to n other silicon atoms. Q^0 refers to monomer of TEOS or silicic acid. For PDMS polymer D refers to Si atom in the chain backbone and $D(Q)$ is the Si atom in copolymer between TEOS and PDMS. As a reference for the different chemical shifts in ^{29}Si NMR spectra, (Table 7) show the corresponding shifts referred to TMS used as reference ($\delta=0$), chloroform as the lock (internal field/frequency control) solvent and chromium acetylacetonate as a non-polar paramagnetic relaxation agent.

On the other hand, rubbery ormosil are potentially a new family of high temperature rubbery materials, the monolithic gel pyrolysed under inert gas flow above 600°C can be converting to a "black glass"⁷⁴. This complex amorphous refractory is a silica-silicon oxycarbide nanocomposite which excellent thermal insulation and low expansion coefficient. Indeed, the thermal stability of the ormosil can also be improved using C_6H_5 groups of the silanol-terminated PDPS.

The good hybridation between TEOS/PDMS system have been used to obtain OIHM ranged from brittle xerogels to soft elastomers⁹⁷, in which a lesser degree of microphase separation was achieved. These hybrids has also been used to encapsulate Rhodamine 6G as a dye molecule reducing the formation of dimers⁹⁸. The use of general organo(alkoxy)-silanes to obtain OIHM are widely exposed in the recent review of Chemistry of Materials²⁶.

SONO-ORMOSIL- Ultrasounds has become a common technique in synthetic chemistry⁷⁶. A number of reactions, especially those in heterogeneous systems, have been shown to give enhanced rates and yields under sonication. Recently, ultrasounds has been applied to polymer synthesis with some success⁷⁸. The cavitation phenomena sets up shear gradients, which stretch out and break the

chain in a non-random process, resulting in a lowering of the molecular weight and polydispersity. A second effect of this enhanced molecular motion is a very efficient mixing and dispersion of multi-phase systems. Price et al.⁸³ describe the effect of ultrasounds on the ring opening of octamethylcyclotetrasiloxane to give silanol-terminated PDMS. Sonication was found to increase the rate of polymerisation over conventional stirring and to give higher molecular weights with lower polydispersities, as it is illustrated in the following Table **8**, always in solution. The action of ultrasounds can be appreciate in the Fig. **7**.

Polymers gels have the particular characteristic that the connecting of the chains resulting from the cross-links gives rise to a permanent elastic modulus. A cross-link in the polymer world is a branch joining two long chains attached by a strong covalent bond.

On the other hand, Geissler et al.⁹⁹ present a study of PDMS gels swollen in different liquids by small-angle scattering. The results permit to establish a two-correlation structure, one governed by the short-range fluctuations which correspond to the size of the blobs and other conducted by the long-range characteristic length, which describes static fluctuations governed by the frozen-in elastic constraints that acts between topologically connected cross-links. To illustrated this model the Fig. **8** shows the normalized SAXS spectra of a PDMS gel swollen in octane at the same concentration ($\Phi=0.173$). An observable difference is remarkable in the low- q region, while the signal of the solution reaches a plateau corresponding to the solution-like component and indicating the absence of any long range structure, the signal of the PDMS gel increase in intensity due to, either by chemical differences between the polymer network and the cross-links, either by differences in the local segment concentration caused by the constraints of the cross-links. The authors fit the experimental curves to a two-correlation function based on a lorentzian for the short-range structure and a squared lorentzian for the long-range one, this last function is based on the Debye-Bueche formalism¹⁰⁰, this model is also discussed on the modern treatise¹⁰¹. The fitting values are summarised in the Table **9**.

One of the systematic studies in the early sono-ormosil process is the study by ^{29}Si RMN in the liquid state as a function of the ultrasonic dose reported by Mackenzie et al^{36,37}. They conclude that the hydrolysis and self-condensation of TEOS took place very quickly after the ultrasonic treatment, as can be observed in the Fig. **9**. Q^n silicon species is defined as $\text{Si}(\text{-O-})_n(\text{-OH})_{4-n}$, n being the number of bridging oxygen. For the first 30 sec, all TEOS monomers (Q^0) were hydrolysed and self-condensation began leading to the growth of the Q^2 and Q^3 species. After that, the Q^3 and Q^4 peaks levelled off, then the intensity of the PDMS, D peak, began to decrease and a new broad peak at -17.5 ppm, D(Q), began to grow. This peak D(Q) has been assigned as Si^* atoms in the copolymerisation unit^{102,103}, that is two bridging oxygen and two Si-CH_3 groups. The increase of the new peak D(Q) run parallel with the decrease of the D one, that is produced after the inflection point of the Fig. **5**. This indicates that the copolymerization of PDMS is produced after the hydrolysis and polymerisation of TEOS. Another characteristic of the ultrasounds action is the absence of cyclic tetramers ($\delta = -19$ ppm) of the break polymer observed when solvent is used (Fig **6**). A schematic model can be seen on the Fig. **10**.

The results on sono-ormosil indicate that inside the cavitation hot-spot cause rapid hydrolysis and self-condensation of TEOS, then copolymerisation together with PDMS chains, without forming cyclic species. Ultrasounds not only cause mechanical mixing but also gives rise to chains breaks, which lead to the appearance of free radicals on the end of the broken chains. Mackenzie et al report other effects of reaction parameters on gelation process in sono-ormosil.^{36,37}, such as the decrease of the gelation time with the increase of the acid catalyst content as well as with the wt% of the PDMS. Therefore, the gelation time increase with water and/or solvent dilution.

Sono-ormosil were found to have higher densities than classic gels as is depicted in Fig **11** and by the results of the Table **10**. Indeed thermal stability was slightly improved by ultrasonic treatment and is believed to be due to the increase in the degree of polymerisation.

On the other hand, specific surface areas lower than $1 \text{ m}^2/\text{g}$ have been measured³⁷ on samples of the so-called hard ormosils once dried at 150°C for

24 hours to remove all the residuals from the pores. However, it has been shown that¹⁰⁴, when heating these hybrid samples at 100°C, pore size distribution and volume are strongly modified with respect to non heat-treated samples. In fact, our experiments on nitrogen adsorption on sono-ormosils samples, previously evacuated at 60°C, show an enlargement of the pores with increasing organic content as well as a decrease in surface areas which can range to hundreds of m²/g, whose results are shown in Table **11**.

In a similar way the corresponding ²⁹Si NMR study for pure silica sonogel¹⁰⁵ is shown in the Fig. **12** where the time evolution of the Qⁿ species is depicted for a sono-sol and for a classic one (without ultrasonic treatment). As can be seen in the first state after an ultrasonic dose of 600 J cm⁻³ for a water/TEOS mixture, the sono-sol consisted of 42% of network forming species Q³+Q⁴, whereas in the corresponding classic sol only a 10% of the species were Q³+Q⁴. This corroborates the influence of ultrasounds in both reaction rates, producing a more complete reticulated network with higher number of bridging oxygen.

Silicon alkoxides are thermodynamically incompatible with the organic silanol-terminated PDMS giving differences in the hydrolysis rate. This fact produces in many cases a phase separation giving an inhomogeneous gel. To avoid this difficulty, the alkoxide+PDMS mixture is previously hydrolysed under the action of ultrasounds (U_s=300 J cm⁻³) with a lower water molar ratio relative to the alkoxide, ranging 0.5 to 0.9 in hard acidic medium. This solution is let one day at 50°C hermetically closed, along this time it evolved into transparent solution suspecting that covalent bonds have been formed between silanol end groups of PDMS chains and the polymerizable Si atoms of the TEOS, that is copolymerisation between organic and inorganic phases. Then hydrolysis reaction is completed by adding the acid water to complete the stoichiometric molar ratio relative to the alkoxide (R=4) and submitted to an additional 500 J cm⁻³ ultrasonic energy dose. The total ultrasonic energy delivered to the solution correspond to the second regime in Fig **5** where dominate the polymerisation of species and start the copolymerisation with the PDMS (see Fig. **9** at 12 min or equivalent to 912 J·cm⁻³ ultrasonic energy dose). Finally the solution is ready either for gelation as an ormosil either to be doped by organic

dyes or semiconductor nanocrystals before gelation. A detailed study of this process is described in the paragraph of optical properties of sono-ormosil⁴⁰. The undoped matrix microporosity can be seen in the Fig **30** (see paragraph quantum dots in the optical properties) from the nitrogen isotherm at 77K where shows a typical feature of a type I isotherm. No hysteresis loop confirm the absence of capillary condensation in mesopores being characteristic of microporous solids (1.05 nm average pore radius).

3.3.- WET SONOGELS.

(degree of reticulation)

The first step in the sol-gel process after gelation is the study of the wet gel, and the important structural evolution during its consolidation, when still is immersed in the mother liquid, a water+alcohol mixture. At this point, one of the most important behaviour of the wet gel is the elastic and viscoelastic properties. Since these properties are very sensitive to the way in which the gel has been prepared and can inform about the degree of solid network reticulation, before any drying process.

As was reported by Zarzycki¹⁰⁶ the ultrasonic energy doses U_s ($J\ cm^{-3}$) has a pronounced effect on the Young's modulus (E) of the wet sonogels. This elastic modulus relates the fractional change in sample dimension produced by a change of pressure, particularly the Young's modulus is obtained by linear tension producing extension. In this way, the elastic modulus $E' = E/(1-\nu^2)$ can be obtained, ν being the Poisson's ratio between the longitudinal and transversal deformation¹⁰⁷. In wet gels, the evaluation of E' is carried out by using the Hertzian contact of a sphere of radius R pressed onto the surface of the gel considered of infinite extent. If a load P induces a deformation d and the elastic behaviour is perfect then:

$$E' = \frac{4 \cdot P}{3\sqrt{R \cdot d^3}}$$

In practice, E' can be obtained from the slope of the linear portion of the $d^{3/2}$ vs. P plot.

Fig. **13** shows the time evolution of the E' values for silica sonogels obtained with different water/TEOS molar ratios and submitted to various ultrasonic doses. As can be seen E' varies strongly with time due to a continuing network crosslinking and syneresis effects, the values level off depends of both water content and ultrasonic dose. This limit value decreases when R increases and differs 1-2 orders of magnitude from the initial value. High water content and low ultrasonic dose slow down the degree of the gel network cross-linking. For fixed water content increasing the ultrasonic dose can bring about a similar effect. Other mechanical parameters as the critical stress intensity factor K_{IC} and the fracture surface energy Γ are measured with the difficulty for the extreme fragility of the wet gels. Results for sonogels are summarised in the Table **12**. Where can be observed the evolution of degree of reticulation however the interfacial surface energy is fairly constant on average 0.05 N m^{-1} . The increase in modulus is too large to be explained simply by loss of the porosity, the difference comes from the increased stiffness of the solid phase in the gel.

Hard sono-ormosils (xerogels)¹⁰⁸.

The ultrasound is used to give concentrated solutions and as a consequence more reticulated solid network as well as unique mechanical properties. The study of such mechanical behaviour is made for TEOS/PDMS system with a water molar ratio of 2 and using iPrOH (isopropanol) as common solvent. The liquid mixture was submitted to an ultrasonic energy dose of 3400 J cm^{-3} , just before to provoke the gelation "in situ". Along this time for different ultrasonic energy doses, several ^{29}Si NMR spectra were recorded, in order to investigate the mechanisms leading to the hard ormosil. They present the elastic moduli and the Vickers hardness for different weight fraction of PDMS. They conclude that the hard ormosil are much harder than the plastics and a little softer than soft glasses, in accordance with the values shown in the Table **13** with regard the Table **14**.

Fig **14** shows the NMR spectra before the formation of the hard ormosil. The spectra can be following by the Table **7** for the different Si atoms environments. Self-condensation of TEOS occurred before copolymerisation

with the silanol-terminated PDMS. Then the decrease of the peak D (380 J cm^{-3}) leading to the increase of the D(Q) and D_{4c} peaks. This last peak (-19 ppm) indicates that PDMS chains are broken due to the ultrasounds forming shorter chains and/or cyclic tetramer, due probably to the presence of the solvent iPrOH. Thus this indicates that hydrolysed TEOS reacted in the middle and in the end of the PDMS chain, as a consequence the peak D(Q) increase and it is totally formed at the end of ultrasonic treatment (45 min equivalent to an energy dose of 3400 J cm^{-3}). Just before gelation D and D_{4c} peaks almost disappeared and only D(Q) remained in the spectrum indicating the total reaction of the PDMS.

Finally the mechanical parameters of the obtained sono-ormosil are shown in the following Table **14**. Authors also describes the use of more complex structures based on the TEOS/TIPT/DMEDES ormosil. This sono-ormosil present an improved mechanical properties as is shown in the following Table **15**.

3.4.- DRY SONOGELS (xerogels and aerogels).

We have combined ^{29}Si MAS-NMR and wide angle X-ray scattering (WAXS) to conduct studies on the structure of dried sonogels. The average number of atoms per length unit situated at a distance r from an arbitrary atom taken as a reference is given by the radial distribution function $\text{RDF}(r) = 4\pi r^2 \rho(r)$, where $\rho(r)$ is the local atomic density. The RDF's first peak position indicates the most probable distance of the first neighbours. In Fig. **15** are represented the sonogel, classic gels and silica glass reduced RDFs. This magnitude represents the deviation of the RDF from an uniform distribution $4\pi r^2 \rho_0$, where ρ_0 is the macroscopic density. The average bond length found was to be 0.164 ± 0.001 nm both for sono- and classic gels, 0.002 nm longer than in vitreous silica. The average atom coordination in silica sonogels is very near from that of the bulk silica glass. (Fig. **15**) shows another important finding was that there is a correspondence between sonogel and silica bulk glass RDF maxima up to r near 1.1-1.2 nm. Beyond this distance this analogy deviates sharply. In the case of

the classic gel it occurs more gradually. This differences were interpreted to mean that sonogels are formed by monosized elementary particles of ~1nm radius, whereas the classic gel is formed by particles with a wide size distribution.

The skeletal density of the solid phase was calculated from the RDF(r). This was evaluated by the maximum entropy method¹⁰⁹. The RDF was found to be compatible with the experimental data and, in particular, with the solid backbone density. The macroscopic atomic density of both sono- and classic silica aerogel was found to be $\rho_0 = 63.0 \pm 0.5$ atom/nm³ (2.09 ± 0.02 g/cm³) and for density of pure silica glass, used as a reference, a value of $\rho_0 = 66.0 \pm 0.5$ atom/nm³ (2.19 ± 0.02 g/cm³) resulted. These differences come from the presence of non-bridging oxygens (NBO) on the pore-matrix interface in the aerogels causing lengthening of the average Si-O bonds¹¹⁰.

A first approximation to the number of NBO was done from the area beneath the first RDF peak, A . This is related to the average number of atoms in the first coordination sphere by¹¹¹:

$$A = \frac{1}{\left(\sum x_x Z_i\right)^2} \sum \sum x_x Z_i Z_j n_{ij} \quad (3)$$

Z_i is the i -element atomic number, n_{ij} are the averaged number of j -type atoms in the first coordination sphere of a j -type atom. n_{ij} is calculated from formulated hypothesis. In this case these hypothesis are that each atom has its bonds satisfied except for a fraction α of O, $0 < \alpha < 1$, i.e., $n_{11} = n_{22} = 0$, $n_{12} = 4$ and $n_{21} = 2 - \alpha$, giving $A = 2.99 - 0.747\alpha$. This expression of A was compared with the experimental values $A_{\text{sono}} = 2.97 \pm 0.10$ and $A_{\text{classic}} = 2.87 \pm 0.10$, giving values of $\text{NBO}_{\text{sono}} \cong 8\%$ and $\text{NBO}_{\text{classic}} \cong 16\%$. According to these values, the sonogel atomic network is more reticulated than classic gels. The sonogel route gives an atomic short-range order near to the bulk silica glass.

These results support the ²⁹Si MAS-NMR (Fig. **16** and Table **16**) results that indicate that the sonogel structure is more crosslinked than gels obtained in alcoholic solution. However, the OH surface coverage calculated assuming a model of non-contacting spherical particles of 1 nm radius BET is several times higher than calculated from N₂ physisorption measurements. This was

interpreted as an important number of OH groups are buried in the sonogel structure¹¹². These hydroxyls are difficult to eliminate, causing difficulties when a full densification to form a glass is intended.

3.5.- NEW TRENDS IN OIHM FROM SONO-ORMOSIL.-

Aerogels from TEOS/PDMS sono-ormosil have been successfully obtained, recent results seem to confirm the hybrid character in these aerogels, that is the organic groups are retained in the sample that can still be considered as an OIHM. We have studied the pyrolysis process in these aerogels from sonogels (550 J cm⁻³), with and without PDMS, in this way the Fig. **17** shows the TGA results for both samples in air and inert atmospheres, as can be seen the organics decompose at 230°C (TGA in air) while the pyrolysis of the PDMS is observable between 700-800°C (TGA inert gas).

4.- PHYSICAL PROPERTIES OF OIHM.

4.1.- MECHANICAL PROPERTIES

ORMOSILS

The use of silane additions to gel-derived silica produces molecular-scale composites via sol-gel processing with improved mechanical properties. These organic-inorganic hybrid materials, referred to above as ORMOSILs, offers interesting possibilities in mechanical strengthening for low processing temperatures of new silica based materials.

A lot of work has been devoted to this subject since Schmidt proposed this new type of hybrids about 15 years ago^{19,113,114,115,116}.

Mackenzie *et al*⁹⁶ described the conditions for the development of various microstructures, the properties of rubbery ormosils and how microstructures

can control its properties. The presence of non-linking organic groups in these materials provides higher stress fracture during processing when comparing to their pure oxide gels counterparts. The rubbery behavior of a sample of ormosil of composition TEOS/PDMS/H₂O/HCl in mole ratios 1/0.08/3/0.3 is shown in Fig.18 (**F18**). The compression strain was higher than 50 %, and compression-release cycles of 500 revealed no change of dimensions. A comparison of the mechanical properties of ormosils and other solids is shown in Table **6**.

The stress-strain relationship for the rubber-like materials was analysed by Hu and Mackenzie¹¹⁷ assuming three different structure models. The first one with all silica gel species separated by PDMS chains, and Model 2 with all silica species connected. The third model combined both structures from Model 1 and Model 2. (Fig. **19**) They interpreted the behavior of TEOS/PDMS = 60/40 Ormosil under external stress, as the result of the coiling of the PDMS chains which will displace the silica units into the pores of the microstructure following Model 1, as shown in Fig 19a. The extremely good compressibility can be explained by the porous structure of this structural model. The structures of Model 2 and Model 3, (Fig. 19b and 19c respectively), on the other hand, have insufficient space for the movement of the silica gel species connected to each other, and are more rigid than the structure of Model 1.

Fracture surfaces analysed by SEM revealed both high compressibility and low fracture strength of this materials is due to the porous structure for materials with high PDMS content. The fracture being initialized on the weakest bonds of PDMS, showing a typical fracture surface of brittle silica gel (Figure **20**).

Hu and Mackenzie¹¹⁸ also revised the correlation between mechanical and structure for Ormosils synthesized with different reaction conditions. They used in its study Silanol-terminated polydimethyl siloxane and tetraethoxysilane (TEOS), with a weight ratio (PDMS)/TEOS of 2/3, and varied the reaction temperature from 25 °C to 70 °C, and the H₂O /TEOS molar ratio from 3 to 6. They also varied the acid catalyst HCl/TEOS ratio from 0.1 to 0.4. As a general

trend it was observed a decrease in bulk density of the Ormosils from $1.09 \text{ g}\cdot\text{cm}^{-3}$ to $0.5 \text{ g}\cdot\text{cm}^{-3}$ when the reaction temperature, water content or the concentration of HCl was increased. The average edge connectivity was used to characterize the structure of Ormosils by SEM, and increased with gelation time. This means that the porosity decreased significantly as the gelation time decreased by lowering HCl, H_2O , or temperature. Table **17** resumes different reaction condition and the properties of several Ormosils and Figure **21** shows the drastic variation of the microstructure with reaction time

The analysis of the stress-strain curves of the different samples showed two distinct regions: a linear elastic, and a non-linear region. Edge connectivity was found to increase as the gelation times did. In this case, an increase for both elastic modulus and fracture strength/unit volume was observed. The mechanical properties decreased when edge connectivity decreased. They attributed this mechanical behavior to the chain movement of PDMS and rearrangement of the ormosil structure, as correspond to the rubbery behavior, which is observed when the structure becomes more open.

It was concluded that the elastic modulus in the Ormosils increased with the edge connectivity, observing a maximum value for Young's modulus of 114 Mpa for the solid material

The influence of the PDMS molecular weight on the glass uniformity and mechanical properties has also been investigated⁹⁷. The PDMS chains were incorporated into silica network by reacting OH-terminated PDMS with TEOS and water in ethanol solution with acid catalyst HCl in a molar ratio $\text{TEOS}/\text{H}_2\text{O}/\text{EtOH}/\text{HCl} = 1/2/2.5/0.048$. Different quoted molecular weights of PDMS were added up to final compositions of 78 wt %. The compositions of synthesized Ormosils are summarized in Table **18**. The higher the PDMS content, the lower the Ormosil rigidity, thus exhibiting a rubbery behavior. A lesser degree of microphase separation was achieved by using PDMS of low

molecular weight. The evolution of the elastic modulus versus PDMS contents and for various PDMS molecular weights is represented in Figure **22**.

Recently, hard coating films based on SiO₂-TiO₂ organically modified silane has been obtained by classical sol-gel techniques via acid catalysis of silica and titania sols¹¹⁹. Silicon (TEOS) and titanium (TIP) alkoxides were used as precursors for the inorganic network and γ -Glycidoxypropyltrimethoxysilane (GLYMO) for the organic phase. Its hardness and Young's modulus, in Fig. **23**, revealed a dependence on the heat treatment temperature which could be related to the carbon and titanium content in the film.

Higher heat treatments leads to an increase in the hardness and Young's modulus of both GTT and GT single layers coatings. TGA analysis showed that organic groups burnt off at 500 °C, resulting in purely inorganic material formation. Lower hardness of GTT above 700 °C were attributed by scanning electron microscopy (SEM) to the existence of microcracks. Also the high hardness measurement of GT sample at 1000°C was related, by means of energy dispersive X-ray spectrometry (EDX), with the existence of some organic residues leading to C-Ti bonding formation.

The measured high hardness observed (9 GPa) of treated films was greater than that expected for ordinary glassy carbon, usually less than 3 GPa, showing some advantage of this type of processing.

HARD SONO-ORMOSILS

The effect of ultrasonic irradiation on the gelation and mechanical properties of TEOS/PDMS Ormosils have been also studied³⁷. This processing way allows the possibility to obtain gels with shorter gelation times and without the addition of solvent. The reaction mechanism of the ultrasonic irradiated Ormosil solution was investigated by liquid state ²⁹Si NMR. The densities of this kind of gels

called "sono-ormosils" were found to be much higher than those without irradiation.

The hardness of these ormosils were measured¹²⁰ and compared with those of the hardest transparent plastics, observing Vickers hardness values six times higher for the ormosil (150 kg mm⁻²). Makishima and Mackenzie,^{121,122} and Yamane and Mackenzie¹²³ developed theoretical models and semiempirically derived equations for the calculation of elastic modulus E, Vickers hardness H_v, shear modulus S and bulk modulus K, considering the packing density and the dissociation energy per unit volume of the oxide constituents, and they are given by:

$$E = 8.36 V_t G \quad (1)$$

$$S = [3.6 V_t (10.8 V_t - 1)] E \quad (2)$$

$$K = 1.2 V_t E \quad (3)$$

$$H_v = 337 [1 (10.8 V_t - 1)]^{1/2} V_t^2 \alpha^{1/2} G \quad (4)$$

where V_t is the packing density and G is the dissociation energy per unit volume of the oxide constituents. V_t is defined as:

$$V_t = \left(\frac{\rho}{M} \right) \sum V_i x_i$$

where ρ is the density, M is the molecular weight, V_i is the packing factor and x_i is the mole fraction of component i , and G is given by:

$$G = \sum G_i x_i$$

where G_i is the dissociation energy per unit volume of component i .

α is the relative bond strength ($\alpha = 1$ for SiO₂ glass) and is given by:

$$\alpha = \frac{\sum f_j n_j \varepsilon_j}{\varepsilon_{Si} \sum f_j n_j}$$

where f_j is the number of cation j in one mole weight of glass, n_j is the coordination number, ε_j is the single bond strength of cation j to oxygen bond and ε_{Si} is the single bond strength of Si-O bond.

In expression (1) E and G are given in Gpa and kcal·cm⁻³, respectively and in equation (4) H_v is given in kg·mm⁻².

Since gels have hydroxyl and alcoxyl dangling bonds and pores, E and H_v for the hard ormosils are expressed as:

$$E = 8.36 C V_t G$$

$$H_v = 337 C \left[1 + (10.8 V_t - 1) \right]^{1/2} V_t^2 \alpha^{1/2} G$$

where C is a constant. G and α are already known and V_t is calculated from the density. Silica sonogel is used as reference to obtain C .

Calculated and experimental values obtained by authors of the elastic moduli and Vickers hardnesses of these TEOS/PDMS hard Ormosils are shown in Fig. **24** a) and b), respectively.

Based on this model, the authors predicted that when Al_2O_3 , ZrO_2 and TiO_2 are substituted for SiO_2 , higher Vickers hardnesses of the hard ormosils are obtained.

The dynamic elastic behavior and its correlation to tailor the mechanical properties of these materials, were studied by means of high resolution Brillouin spectroscopy^{92, 93, 104}. This technique was applied before to the study of the fundamental aspects of viscoelastic and elastic properties of a broad range of amorphous materials. PDMS with an average molecular weight of 550 was used and its content varied from 0 to 40 wt % referred to TEOS. The ultrasonic energy submitted to the start solution was 0.12 kJ cm^{-3} . Description of the technique employed to measure the mechanical properties can be found in the mentioned article and therein references. From measured dynamic and hypersonic properties, the elastic pure longitudinal mode constant c_{11} ¹²⁴ was extracted, and a structural model for the ormosils inferred depending on the PDMS content. The proposed structure agrees with NMR data from previous studies³⁷ for these materials. It is resumed in the fact that as the molar fraction of PDMS increases, the probability of breaking the polymer chain by TEOS decreases, and autocondensation of PDMS is more feasible.

4.2.- OPTICAL PROPERTIES

ORMOSILS

Both the transparency and mechanical improvement that Ormosils offers respect to other gels, have been exploited extensively for more than ten years ago, as it is revealed by the numerous studies which have been published in specialist journals devoted to these subjects.

One of the former studies was dedicated to the incorporation of various organic laser dyes into ormosils¹²⁵ derived from TEOS and PDMS. The machining for optical purposes of these materials are favoured prior to heat treatment, due to

its lower porosity and enhanced mechanical properties. Also, organic functionalities offers a great flexibility with respect to chemical compatibility of the gels with the dye to be incorporated. They exhibited high optical transmission and considering optical gain behave as better hosts for organic dyes than polymethyl methacrylate (PMMA), and are comparable with liquid methanolic alcohol solvent. Rhodamine 610 exhibited higher optical gain (10.9 cm^{-1}) even than in methyl alcohol (9.2 cm^{-1}) as shown in Fig. **25**. The degradation of the optical gain with time was also reduced for ormosil matrices, and stability of the organic dyes were in some cases higher than in methyl alcohol. The optical gain of various dyes Rh6G, Rh610, Rh620, and C540, in different host media Ormosils, PMMA and methyl-alcohol are listed in Table **19**.

Non-linear optical properties of dye-doped hybrid and nanoparticle ormosil materials have been also investigated in the last years. The low temperatures involved in the sol-gel processing combined with the improvement of ormosil properties to support secondary phases with interest in optics, are the main reasons for the observed extensively developing in this research area. Gan¹²⁶ has studied for the first time the optical limiting effect of fullerene doped Ormosil and the photoinduced and electroinduced second harmonic generation of CuI, Sb_2S_3 and Bi_2S_3 nanoparticle doped gels and glasses, showing that this sol-gel derived materials have potential applications in the fields of optics and optoelectronics.

Optical nonlinearity of nanocomposite materials can be increased by increasing particle concentration, which is quite suitable from the sol-gel method, by adding dielectric confinement beside the quantum confinement effect or by working at near-resonant wavelength. Thus, for example, when comparing third-order nonlinear susceptibility $\chi^{(3)}$ from 2% CdS glass with 8 % CdS sol-gel derived nanocomposite¹²⁷, it varied from 1.5×10^{-10} esu at 390 nm to 6.3×10^{-7} esu.

There is also great interest for applying the hybrid approach to obtain waveguides with low optical losses. Recently, SiO₂-TiO₂ waveguides have been obtained from titanium alkoxide precursor sol containing an organically modified alkoxide, such as methyltriethoxysilane¹²⁸. The advantage of the hybrid materials is that multimode waveguides are obtained and, because of the lower temperature required for processing (around 150 °C), can be used as hosts for optically active organic molecules.

In order to determine the requirements to reduce the optical loss for waveguides made from ormosil films, based on trimethoxysilyl-propylmethacrylate (TMSPM) organic modified alkoxide, Near-infrared (NIR) and mid-Infrared (MIR) spectroscopy has been used¹²⁹. The reported results in that work signalled that the films must be protected in dry atmosphere or cover coating to protect them from adsorption of water, which absorbs at around 1.55 μm, which is one of the signal wavelengths used for optical communications.

Ormosil systems makes the variation of refractive index feasible by modification of the silica network with different organic groups. In this sense a recent work¹³⁰ reported refractive index variations ranging from 1.40 to 1.55 in ormosil films. The starting materials used were methyl triethoxysilane (MTES) and phenyl triethoxysilane (PhTES) and tetraethyl orthosilicate TEOS. The study indicates that the refractive index of PhTES/TEOS films increases sub-linearly with increasing phenyl content up to approximately 1.55. (Fig. **26**). This behavior is assigned by the authors to the high polarisability (π -bonding electrons), of phenyl groups combined with the observed decrease in density arising from steric effects in agreement with Vorotilov et al.¹³¹. As expected, replacing the highly polarisable phenyl groups with methyl groups reduces the refractive index, while maintaining the overall organic content of the organic material, as can be observed in Fig. **27** a) and b). Resistance to cracking during the drying process depends strongly on the composition, and films with thickness up to 15 μm were dried crack-free at temperatures up to 200 °C. Drying decreases the refractive index for all compositions except those with a

high phenyl content, which showed a slight increase (up to 0.006 for 100 % PhTES film). The study has also shown that ormosil materials comprising phenyl- and methyl-substituted silica have several promising properties for photonic applications.

SONO-ORMOSILS

Organic Dyes.

Ultrasonic cavitation has also been applied to the preparation of the aforementioned second type of hybrid materials. For effective entrapment of organic molecules a stable and transparent sol-gel matrix is required with a narrow pore size distribution. This minimizes light dispersion effects and induces an uniform cluster size distribution of the guest ¹³². In this way, several organic dyes were effectively trapped in the sono-xerogel pores, by adding the optically active phase in the sol step, leading to very stable copposites for optical applications ^{133, 134}. The most promising results were obtained by encapsulating copper phthalocyanine (CuPc), which is a macrocyclic planar molecule with extended π -electron delocalisation that gives rise to extremely large molecular second order hyperpolarizabilites causin third-order nonlinear optical processes ¹³⁵.

The effectiveness of the proposed route for trapping this molecular phase (CuPc) in a sonogel was examined by UV-VIS absorption at different stages of processing, from the starting sol to the dried composite ¹³⁴. The typical Q absorption band is broad and split with two maxima at 692 and 614 nm in all the curves. The band position and the with indicate the coexistence of monomeric and aggregated species. In contrast, the increase in composite optical density with time, due to the higher PC concentration in the shrinking inorganic network implies effective molecule trapping in the host matrix. The absorption spectra of leachable liquids do not show any evidence of the Pc-Q band.

The non-linear optical behavior of the encapsulated molecules has been checked by various tests. The distortion of a 532 nm Nd:YAG laser beam profile after propagation through samples was analyzed and Fig. **28** is an example of the transmitted profiles obtained. Strong self-defocusing effects appear in samples with CuPc concentrations between 10^{-5} and 10^{-4} M⁹⁰, revealing an intensity-dependent refractive index for the doped sonogels.

The non-linear absorption dispersion was studied by Z-scan¹³⁶. This technique measures the total laser energy transmitted through the sample. This is given as a sample position function along the optical axis with respect to the focal plane. The results indicate that the sign of the non-linear optical refractive index changes near 550 nm. However, to enhance the magnitude and spectral characteristics of the negative refractive index range in the composite, the processing should lead to a monomer/aggregate ratio that is as high as possible.

Quantum dots.

Solventless ormosils prepared by sonocatalysis exhibit suitable features to incorporate and provide uniform sized quantum dots. Among others, shorter gelation times, higher matrix densities, smaller pore radii, and narrower pore size distribution than those obtained from classic gels^{36,87}. As a consequence, thermal and mechanical stability of the resulting sonogels and sono-ormosils are improved in relation with other kind of gels^{37, 22}, used as host matrices for supporting dispersed semiconductor nanoparticles.

A recent study on the stabilisation and control growth of PbS quantum dots (QDs) stabilized with surface-capping agents (SCA), incorporated into rigid transparent SiO₂ sono-ormosil has been reported⁴⁰. In this work, silanol-terminated PDMS with quoted average molecular weight of 400-700, and TMOS, were used for preparing the hybrid organic-inorganic host matrices.

Using ultrasonic irradiation to form "sono-ormosils" shortened the chemical reactions between both organic and inorganic precursors. In order to ensure the homogeneous incorporation of PDMS chains into the silica inorganic network, a two-step acid catalysed hydrolysis was used and described in the same reference.

The chemical route for the preparation of the host gel and composites proposed is schematised in Fig. **29**. The resulting sol A was translucent due to sub- micro or even nanophase separation, as a result of thermodynamic incompatibility between the organic and inorganic precursors. Furtherly, it was kept at 50 °C for 24 hours and, along this time, it evolved into transparent solution suspecting that covalent bonds have been formed between silanol groups of PDMS chains and the inorganic constituent.

The nucleation of PbS was helped by adding suitable amounts of lead acetate (PbAc_2) and mercaptopropyl trimethoxysilane (MPTMS) which acts as SCA agent to promote a high dispersed dot population, and in order to test its influence on the further control growth of the colloidal particles of PbS.

Table **20** resumes the molar ratios used in the outlined samples. The code sample is referred as XRY, X being the nominal PbS wt % and Y the MPTMS/Pb molar ratio. Finally thioacetamide (TAA) was added into the matrix solution to obtain the respective PbS wt %.

The gel transition was accelerated by adding ammonia methanolic solution. By this way, yellow coloured gels were obtained which turn progressively into orange, red, brown and black coloured transparent gels. All of the samples were heat-treated up to 100°C at 1°C/min for 3 hours in N_2 atmosphere, to avoid decomposition of PbS to form the corresponding oxide PbO.

To elucidate the microstructure of the resulting PbS doped-ormosils, thermogravimetric analysis (TGA), x-ray diffraction (XRD) and N_2 -physisorption isotherms at 77 K were performed on these samples. From their results it was deduced that PbS cubic nanocrystals were homogenously distributed and embedded into a microporous silica matrix and stabilized at 100 °C. As observed in Fig. **30**, the N_2 -adsorption curves show the typical features of a type I isotherm, characterized by a knee at low relative pressure ($P/P_0 < 0.2$) and a horizontal plateau in almost whole the relative pressure range with a sharp increase near saturation pressure. No hysteresis loop is noticeable; this is the typical signature of microporous solids by the absence of capillary condensation in mesopores. The textural parameters evaluated from the N_2 isotherms are summarized in Table **21**. A decrease in the specific surface area

with an increase in the PbS content is observed. The correlation coefficients correspond to the linear regression of the BET equation. This behaviour could be due to some differences in pore sizes as a consequence of the steric effects coming from the non-bonded 3-mercaptopropyl groups, since they are electrostatically opposite to the silica network. This assumption is confirmed by the good agreement existing between the apparent densities calculated from the porous volume and from the geometrical dimensions. Bulk density (ρ_s), were evaluated taking into account the corresponding weight percent in the composite $(\text{SiO}_2)_{1-x}-(\text{PbS})_x$ by using $2.2 \text{ g}\cdot\text{cm}^{-3}$ for vitreous silica and $7.5 \text{ g}\cdot\text{cm}^{-3}$ for PbS. Finally, average pore sizes in the last column corroborate the fine porosity of the host matrix.

The observation of the samples by using an High Resolution Transmission Electronic Microscope (HRTEM) allowed the calculation of the particle size distribution for PbS which were identified by electron diffraction techniques thus confirming the results from XRD (Fig. **31**).

Finally, optical absorption measurements in the 300 nm to 1200 nm range with an ultraviolet-visible-near-infrared spectrometer showed the typical blue-shift due to the quantum confinement of the exciton in the PbS nanocrystals, and concluding that higher SCA contents provoked the absence of subbanding as well as a long tail in the absorption in the curves, attributed to the interface-related trap processes located at the boundary of the crystal surface with the dielectric matrix (Fig. **32**)

Additionally, the analysis of the structure of these materials was completed by Small Angle Neutron Scattering techniques (SANS)¹³⁷. It revealed the existence of residual elastic strains in the network due to polymer cross-links, as well as crystal sizes in the confinement regime of PbS.¹³⁸ Normalized intensities were analysed by calculating, with the aid of suitable models, the form factor $P(q)$ and the structure factor $S(q)$, according to $I(q) = (\Delta\rho)^2 N P(q) S(q)$, N being the number density and $\Delta\rho$ the contrast difference between the scatters and the surrounding media. For the data analysis a two-correlation length model for the particle scattering factor was assumed, incorporating the Percus-Yevick hard-sphere model to calculate the structure factor.

This model agrees with the existence of PbS core-shell aggregates of 15-75 nm ranging diameter size, homogeneously distributed in a microporous matrix with mean pore size of 0.5 nm. (Fig. **33**)

The short-correlation length, a_2 , calculated represents well the microporosity of the sono-ormosil, the pore size varying from 0.36 nm (1R10) to 0.77 nm (0.25R20). These values agrees well with the corresponding results obtained from adsorption techniques. The Percus-Yevick hard sphere diameter, ξ , combined with the evaluated long correlation length, a_1 , gives rise to a satisfactory description of the microstructure of this kind of materials. This is constituted by a microporous matrix where the PbS nanoparticles are embedded. They are surrounded by SCA molecules and a depleted region where crystal growth is inhibited, forming a core-shell aggregate of 12.27 nm (0.25R20) to 74.7 nm (0.5R64) size. These values are overestimated, due to polymer cross-linking between the aggregates. They are separated by a correlation distance, δ of 28 nm in the case of the sample PbSEDTA1, where ethylenediaminetetraacetic acid (EDTA) instead of MPTMS was used for chelating Pb^{2+} ions, and with a PbS content being similar to that from the 1R10 sample. This correlation distance increased up to 124 nm, for the 4R5 sample.

ACKNOWLEDGEMENTS- Authors thank to the Spanish Ministry of Science and Technology for financial support by the project MAT2001-3644. Authors belong to the TEP-115 research group of the Junta de Andalucía (Spain).

Physical properties of amorphous/vitreous silica (SiO₂).

MW	ρ (g·cm ⁻³)	m.p. (°C)	T _g (°C)	n	Si-O strength (kcal mol ⁻¹)	Young's modulus E (N·m ⁻²)	Shear modulus G (N·m ⁻²)
60.08	2.2	1600	1500-2000	1.458	106	7.2·10 ¹⁰	3.15·10 ¹⁰

Poisson's ratio ν	Fracture surface energy γ (N·m ⁻¹)	Fracture toughness (MN·m ^{-3/2})	Specific volume (m ³ ·kg ⁻¹)	Heat capacity Cp (J·kg ⁻¹ ·K ⁻¹)	Thermal expansion coefficient α (K ⁻¹)	Thermal conductivity K _T (W·m ⁻¹ ·K ⁻¹)
0.17	4.37 (300K)	0.794 (300K)	4.35·10 ⁶	8.00	2.67·10 ⁸	12.85·10 ³

pH	Solubility in water (25°C) ppm
6-8	120
9	138
9.5	180
10	310
10.6	876

Adjusted with HCl or NaOH

Alcohol	Solubility (25°C) ppm
Methanol	1890
Ethanol	164
n-Propanol	8

pH	Activation Energy for gelling (kcal·mol ⁻¹)
4.0	15.0
5.5	14.5
7.0	11.9

Physical properties of typical tetralkoxysilanes

Name	MW	bp	$n_D(20\text{ }^\circ\text{C})$	$d(20\text{ }^\circ\text{C})$	η (cstks)	Dipole Moment	Solubility
TMOS	152.2	121	1.3688	1.02	5.46	1.71	alcohols
TEOS	208.3	169	1.3838	0.93	-	1.63	alcohols

Physical properties of low M.W. Silanol terminated Polydimethylsiloxanes

Code	Viscosity	MW	% (OH)	m.p.($^\circ\text{C}$)	Specific gravity	Refractive index
DMS-S12	20-35	400-700	4.0-6.0	>205	0.95	1.401
DMS-S15	45-85	1500-2000	0.9-1.2	>205	0.96	1.402

Physical properties of Silanol terminated Diphenylsiloxane

Code	Viscosity	Mole % Diphenylsiloxane	% (OH)	M.W.	Refractive index
PDS-1615	50-60	14-18	3.4-4.8	900-1000	1.401

Table 1. Comparison of Vickers hardness among glasses, Sono-orosils and hard transparent polymers.

Material	Vickers Hardness (kg/mm^2)
SiO_2	635
$\text{Na}_2\text{O-CaO-SiO}_2$	487-620
$\text{Ba}_2\text{O}_3\text{-SiO}_2$	227-345
Sb_2O_3	160-215
Sono-Ormosils (≤ 10 wt % PDMS)	88-186
As_2Se_5	105
Polyethyleneterphtalate (PET)	24
Polymethylmethacrylate (PMMA)	19
Polycarbonate (PC)	14-16

Table 2.- Technical data of some ultrasonic horn type apparatus

	UMont.	UCA	UCLA
Apparatus	Meaux-Sonic	Kontes	Fisher
Output power(W)	15	60	70±5
tip diameter (mm)	20	13	8

UMont- University of Montpellier (Zarzycki's group)

UCA- University of Cadiz (Esquivias' group)

UCLA- University of California Los Angeles (Mackenzie's group)

Table 3.- K values from the Table 2 apparatus

	UMont	UCA	UCLA
K(W cm ⁻³)	90	103	76

Table 4.- Threshold and limiting of the ultrasonic energy dose.

U _s (J cm ⁻³)	TEOS/water 4	TEOS/water (PDMS) 2	TMOS/water 4	TMOS/water (PDMS) 2
U _s (min)	80	60	70	40
U _s (max)	1360	1100	350	1000

Table 5. Comparison between rubbery Ormosils and a commercially available rubber

	Ormosil (A) (1/0.08/0.3/3) [#]	Ormosil (B) (1/0.08/0.1/3)	Commercial Sample
Density (g/cc)	0.7-0.8	0.85-0.9	1.08-1.1
Young's modulus Mpa	12-25	60-80	0.95-1.1
Tensile strength Mpa	3-6	10-12	~20
Elongation, %	15-25	8-11	750-850
Resilience, %	15-25	40-50	35-38
Compressive strength, Mpa	25-34	40-45	-
Compressive ϵ_f , %	50-60	15-20	>70

[#] (1/0.08/0.3/3) refers to the molar ratio of (TEOS/PDMS/HCl/H₂O)

Table 6. Mechanical properties of ormosils and elastomers

	Elongation ϵ (%)	Strength σ (Mpa)	Modulus E (Mpa)
Silica gel	minimal	1.38	1.2
Fused silica	0.1	70	7×10^4
PDMS (40 wt%)-TEOS (60 wt %)	3-15	2-3	45-65
PTMO (50 wt %)-TEOS (50 wt %)	113	2.1-6.1	2.8-6.7
Epoxy Si(OR) ₃ -Ti(OR) ₄ (5-20 mol%)		2.1-3.6	2900-3400
Silicon rubber (peroxide cured)	500	8.2	1.7
Polyurethane rubber (termoplastic)	730	36.5	3.1

Table 7. Relationship between ²⁹Si chemical shifts (- δ ppm) relative to liquids TMS and silicate structures

	$-\delta$ ppm	Silicate structure
M ^{OR}	10.2-13.7	RO-Si*(CH ₃) ₂ -OSi≡
D(Q)	15.9-18.0	(-O-) ₃ Si-O-Si*(CH ₃) ₂ -O-Si≡
D _{4c}	18.9-19.6	[Si*(CH ₃) ₂ -O-] ₄ (cyclic)
D	20.1-22.0	-Si(CH ₃) ₂ -O-Si*(CH ₃) ₂ -O-Si(CH ₃) ₂ -O-
Q ⁰	81.0-82.0	Si*(-OR) ₄
Q ¹	85.0-89.0	Si*(-OR) ₃ (-O-Si≡)
Q ²	88.0-94.0	Si*(-OR) ₂ (-O-Si≡) ₂
Q ³	96.0-104.0	Si*(-OR)(-O-Si≡) ₃
Q ⁴	106.0-110.0	Si*(-O-Si≡) ₄

Each peak shows Si*. R = H or C₂H₅

Table 8.- The effect of ultrasounds intensity on the preparation of PDMS^a

Ultrasounds intensity	Molecular weight	Polydispersity	Conversión(%)
18	24 200	1.6	63
23	31 000	1.6	64
32	44 300	1.9	73

A Reaction conditions: 90 min using ultrasounds horn at 18°C with 1 cm³ H₂SO₄ catalyst. Intensities in W cm⁻².

Table 9. Fitting parameter for equation (5) for PDMS gels

Solvent	ϕ	ϕ ($\partial\phi/\partial\Pi$) (kPa)	B (kPa)	ξ (Å)	Ξ (Å)
Octane	0.173	$2.70 \cdot 10^{-4}$	$2.63 \cdot 10^{-3}$	20.0	53.9
	0.238	$1.74 \cdot 10^{-4}$	$1.65 \cdot 10^{-3}$	13.3	51.2
	0.287	$1.50 \cdot 10^{-4}$	$1.25 \cdot 10^{-3}$	11.9	51.5

Table 10. Evolution of densities and BET results of sono-Ormosils compared to those of sonogel without ultrasonic irradiation (H₂O/TEOS (mol/mol) = 2, HCl/TEOS (mol/mol) = 0.05

	Composition of the starting materials							
	Sonogel	Sono-Ormosils			Classic gels*			
PDMS/TEOS (wt/wt)	0/100	10/90	20/80	40/60	0, .00	10/90	20/80	40/60
Density (g/cm ³)	1.78	1.46	1.26	0.96	<1.62	<1.33	<1.14	<0.89
Specific surface area (m ² /g)	≈ 200	<1	<1	<1		200-800		
Porosity (%)						20-50		

The wide range of the data are due to the variety of controlling factors, such as solvent, aging, temperature, evaporation rate, etc.

Table 11. Textural parameters of hybrid samples heated at 100 °C

DMS (molar %)	Bulk density (g·cm ⁻³)	Skeletal density (g·cm ⁻³)	S _{BET} (m ² ·g ⁻¹)	V _P (cm ⁻³ ·g ⁻¹)
24	1.39	1.45	350	0.20
40	1.14	1.32	372	0.27
55	1.07	1.18	220	0.24
65	1.17	1.17	--	0.18

Table 12. Mechanical characterisation of SiO₂ wet sonogels

Irradiation dose (J·cm ⁻³)	Aging time (h)	K _{IC} (N·m ⁻²)	E' (N·m ⁻²)	Γ (N·m ⁻¹)
450	24	162	2.6 x10 ⁶	0.049
300	53	246	6.0 x10 ⁶	0.050
800	20	277	6.2 x10 ⁶	0.062
600	40	279	9.0 x10 ⁶	0.043

Table 13. Vickers hardnesses of some glasses and the hardest transparent plastics

Material	Vickers hardness (kg/mm ²)
Polyethyleneterephthalate (PET)	24
Polymethylmethacrylate (PMMA)	19
Polycarbonate (PC)	14-16
Borosilicate glass	220-350
Window glass	480-620

Table 14. Bulk densities, elastic moduli and Vickers hardnesses of the TEOS/PDMS system hard ormosils

Weight fraction of PDMS	0	0.03	0.05	0.08	0.10	0.12	0.15
Mole fraction of [Si(CH ₃) ₂ -O-]	0	0.079	0.128	0.195	0.237	0.275	0.329
Bulk density (g/cm ³)	1.78	1.65	1.59	1.50	1.46	1.41	1.36
Elastic modulus (Gpa)	20.7	18.6	16.0	15.0	13.0	11.7	11.0
Vickers hardness (kg/mm ²)	186	160	140	110	88	83	76

Table 15. Bulk densities, elastic moduli and Vickers hardnesses of 30 mol% TiO₂-containing hard ormosils

Mole fraction of DMDES	0	0.05	0.10	0.15	0.20	0.25	0.30
Bulk density (g/cm ³)	1.96	1.87	1.78	1.70	1.63	1.57	1.52
Elastic modulus (Gpa)	23.0	22.0	18.1	17.2	16.4	14.2	12.6
Vickers hardness (kg/mm ²)	211	179	155	150	130	110	106

Table 16. ^{29}Si NMR analysis and specific surface area

Sample	Q^2 (ppm)	Q^3 (ppm)	Q^4 (ppm)	$Q^2:Q^3:Q^4$	$n_{\text{OH}}/n_{\text{Si}}$	$\phi(^{\circ})$	$S(\text{m}^2 \text{g}^{-1})$
S2	-89.3	-100.1	-109.3	12:27:61	0.51	145.4	640
S6	-88.4	-99.2	-109.1	15:35:50	0.60	145.0	777
S10	-90.0	-99.8	-108.8	10:28:62	0.48	144.6	380
S14	-88.3	-99.5	-109.3	7:27:66	0.41	130.1	-
C2	-90.0	-99.7	-108.3	6:40:54	0.52	143.9	700
C6	-88.6	-100.1	-111.5	10:35:55	0.55	149.1	693

Table 17. The reaction condition for and the properties of several Ormosils

Sample number	Reaction Temperature ($^{\circ}\text{C}$)	HCl/TEOS molar ratio	$\text{H}_2\text{O}/\text{TEOS}$ molar ratio	Average Bulk Density (g/cm^3)	Open porosity (%)
1	25	0.3	3	1.09	6.5
2	40	0.3	3	0.91	17.3
3	50	0.3	3	0.83	26.8
4	60	0.3	3	0.65	40.9
5	70	0.3	3	0.56	49.5
6	60	0.1	3	1.10	1.9
7	60	0.2	3	0.88	19.2
8	60	0.3	3	0.65	40.9
9	60	0.4	3	0.50	54.5
10	70	0.3	2	0.72	33.9
11	70	0.3	3	0.56	49.5
12	70	0.3	4	0.50	54.1
13	70	0.3	5	0.48	56.4
14	70	0.3	6	0.49	55.8

Table 18. Summary of synthesized Ormosil compositions and final appearance (T: transparent; o: slightly opaque; O: opaque)

Experimental wt. ratio PDMS/TEOS	0	1/99	1/49	1/19	7/93	1/9	15/85	1/4	3/7	2/3	1	
PDMS theoretical wt % In final Ormosil	0%	3%	7%	15%	21%	28%	38%	46%	60%	70%	78%	
PDMS quoted molecular weight	550	T	T	T	T	T	T	T	T	o	O	O
	4200	T	T	--	T	T	--	O	O	O	--	
	18000	T	T	--	T	T	--	O	O	O	--	
	43500	T	T	T	T	T	O	--	O	O	O	--

Table 19. Optical gain of organic laser dyes in Ormosils, PMMA, and methanol.

		Dye ^a				
		C540A 540	Rh6G 590	Rh610 610	Rh620 620	Rh640 640
Ormosil	conc. (mol ⁻¹)	1.0 x 10 ⁻³	1.0 x 10 ⁻³	3.2 x 10 ⁻³	1.0 x 10 ⁻³	1.0 x 10 ⁻³
	gain (cm ⁻¹)	1.2	10.5	10.9	7.8	3.9
PMMA	conc. (mol ⁻¹)	5.0 x 10 ⁻⁴		5.0 x 10 ⁻⁴	5.0 x 10 ⁻⁴	5.0 x 10 ⁻⁴
	gain (cm ⁻¹)	0.7		1.7	2.1	1.9
Methanol	conc. (mol ⁻¹)	3.2 x 10 ⁻³	3.2 x 10 ⁻³	3.2 x 10 ⁻³	3.2 x 10 ⁻³	3.2 x 10 ⁻³
	gain (cm ⁻¹)	7.0	10.0	9.2	8.7	8.0

^a Rh, rhodamine; C, coumarin.

Table 20. Molar ratios respect to TMOS of the reactive precursors used in the preparation of PbS-Ormosils. The PDMS was added in a 10 % of volume ratio to TMOS volume in the four samples signaled.

Sample	PbAc ₂	MPTMS (x 10 ⁻³)	TAA
0.5R32	1.35	41.6	1.8
1R10	2.7	26.0	3.6
4R5	10.8	52.0	14.4

Table 21. Specific surface area (S), Pore volume (V_p) and apparent density (ρ_a) calculated from N₂ physisorption data. The apparent density (ρ) evaluated from geometrical measurement and the pore size from cylindrical pores.

Sample	S (corr. coeff.) (m ² ·g ⁻¹)	V _p (cm ³ ·g ⁻¹)	* ρ _a (g·cm ⁻³)	** ρ geometric (g·cm ⁻³)	Pore size (nm)
Undoped matrix	616 (0.9994)	0.324	1.28	1.29 ± 0.05	2.10
0.5R32	677 (0.9989)	0.483	1.07	1.03 ± 0.05	2.86
1R10	542 (0.9990)	0.468	1.09	1.08 ± 0.05	3.46
4R5	414 (0.9978)	0.210	1.56	1.55 ± 0.05	2.02

$$* \frac{1}{\rho_a} = V_p + \frac{1}{\rho_s}$$

** parallelepiped casting.

Figure 1. Schematic process of the high power ultrasounds treatment.

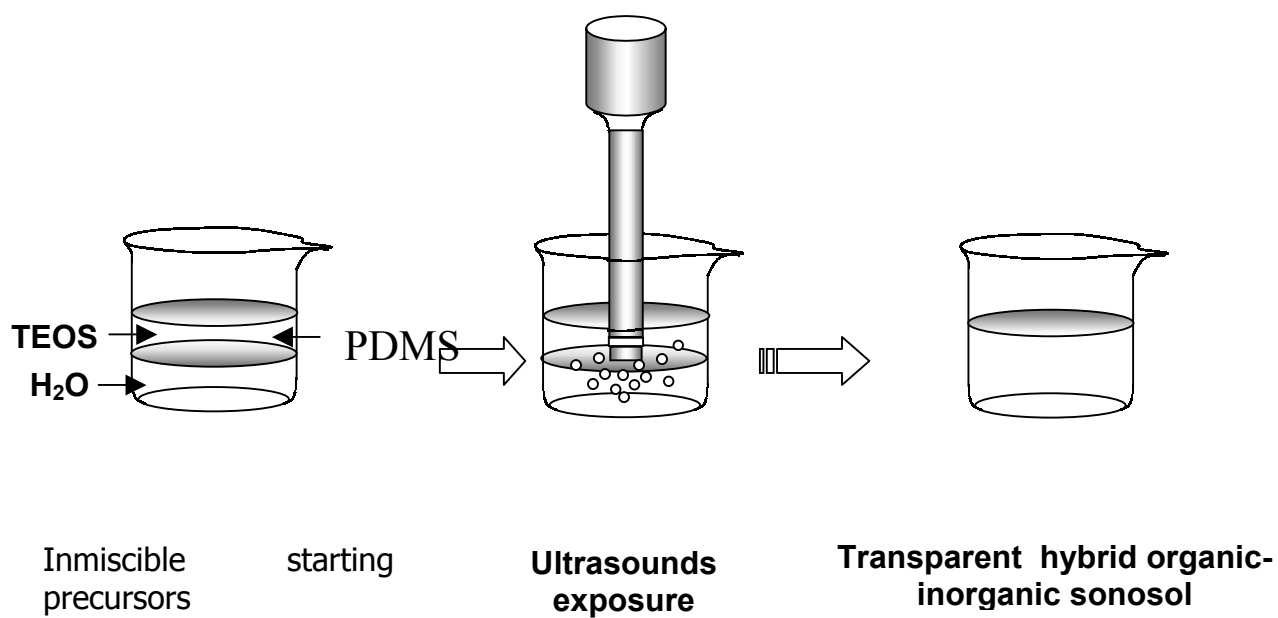


Figure 2. Change in temperature of the solution during the ultrasonic treatment

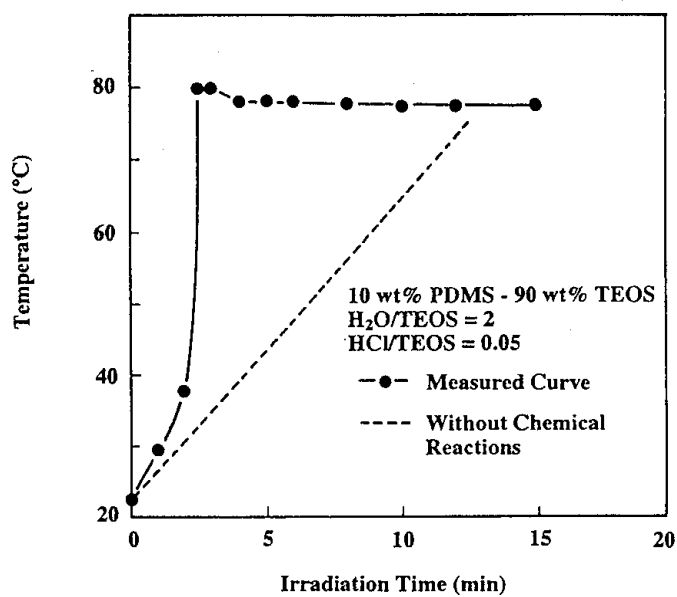


Figure 3. Evolution of the gelation time for Water/TEOS=4 pure sonogels in function of ultrasonic energy doses at different temperatures.

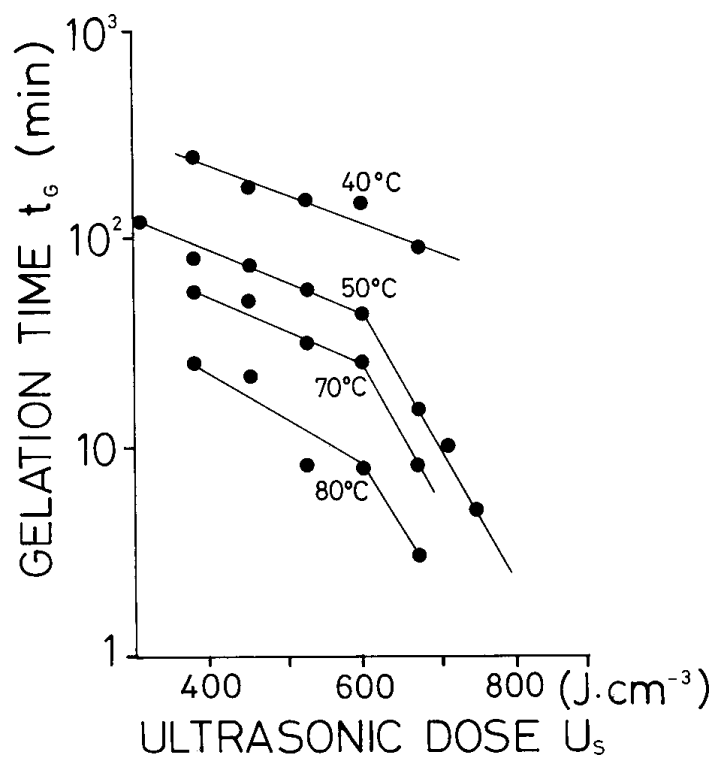


Figure 4. Evolution of the gelation time for water/TEOS=4 pure sonogels in function of 1/T for different ultrasonic energy doses.

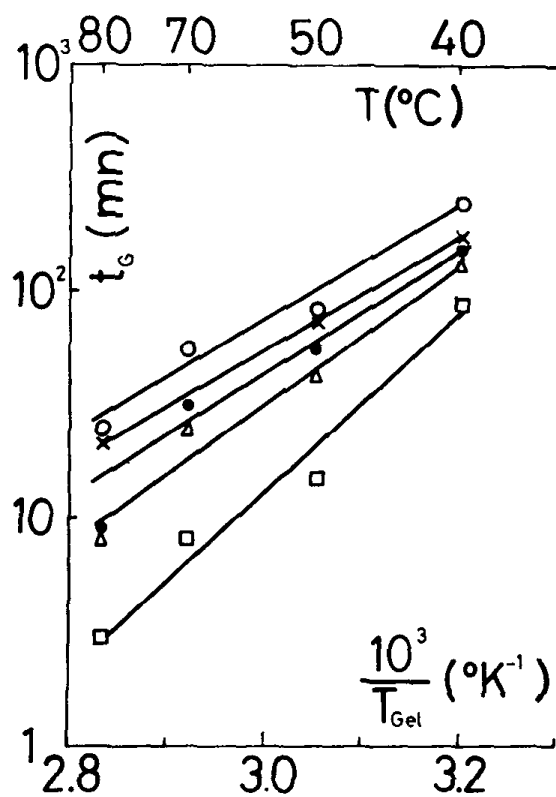


Figure 5. Evolution of the gelation time for water/TEOS=2 and 10wt%PDMS-90wt%TEOS in function of the ultrasonic energy doses. Arrow indicates the inflexion point between the two regimes.

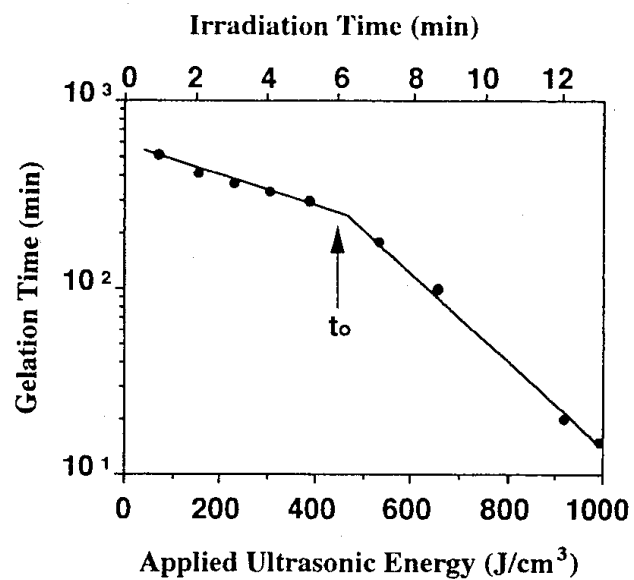


Figure 6. ^{29}Si NMR spectra of solution gel concentration (TEOS/PDMS/ $\text{H}_2\text{O}/\text{HCl}$)=(1/0.08/3/0.1) in function of the chemical shift using TMS as reference signal, at different reaction time.

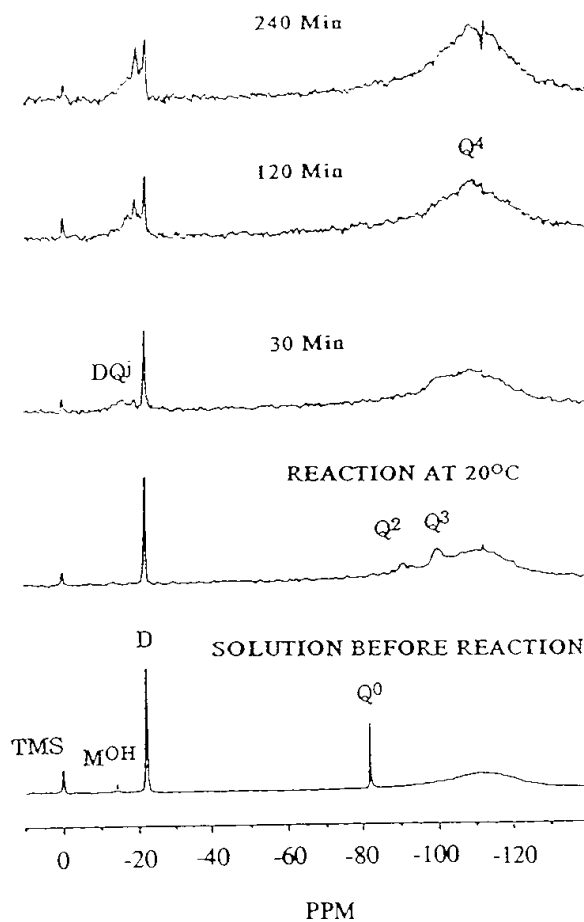


Figure 7. Influence of the ultrasounds in the preparation of PDMS at 25°C.

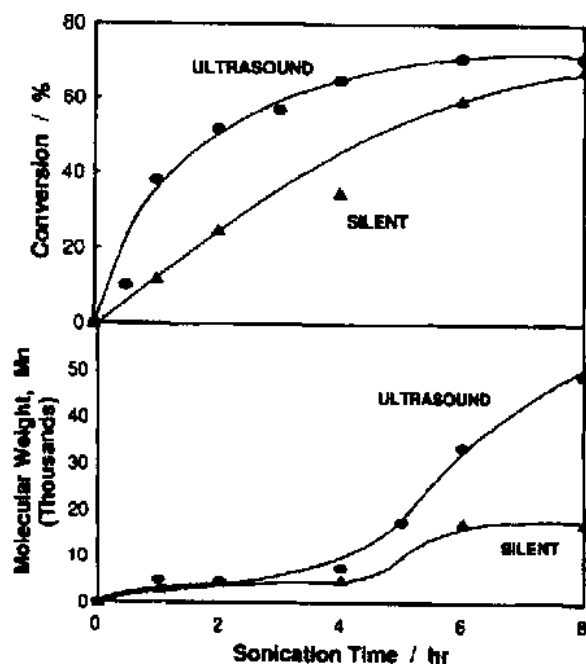


Figure 8. SANS spectra of PDMS gel in octane at $\Phi=0.173$ into liquid-like (continuous line) and solid-like components.

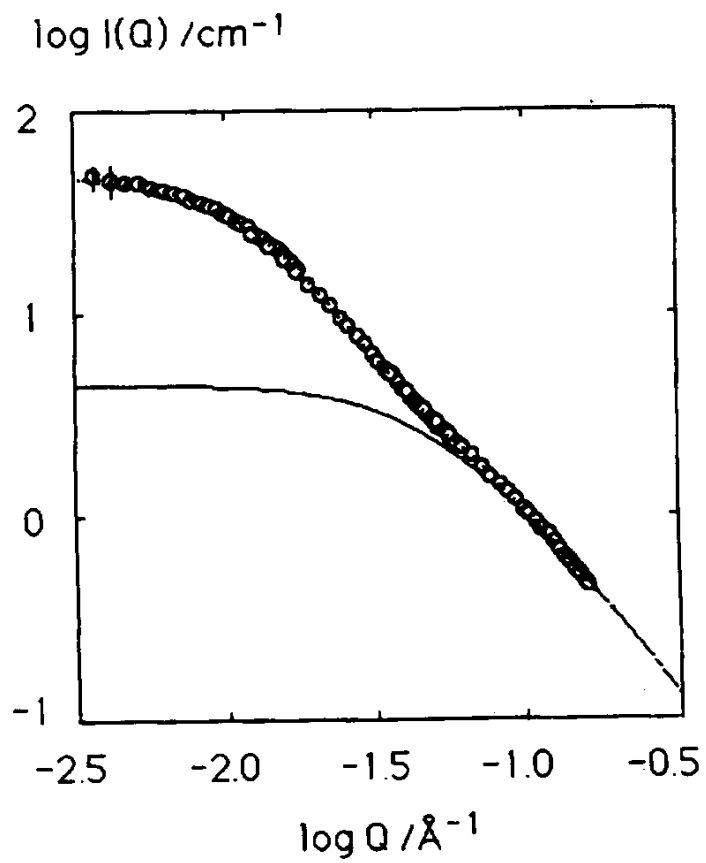


Figure 9. ^{29}Si NMR spectra of 10wt%PDMS-90wt%TEOS solution for different ultrasonic energy doses ($U_s=76 \text{ t (J}\cdot\text{cm}^{-3})$ time in min.

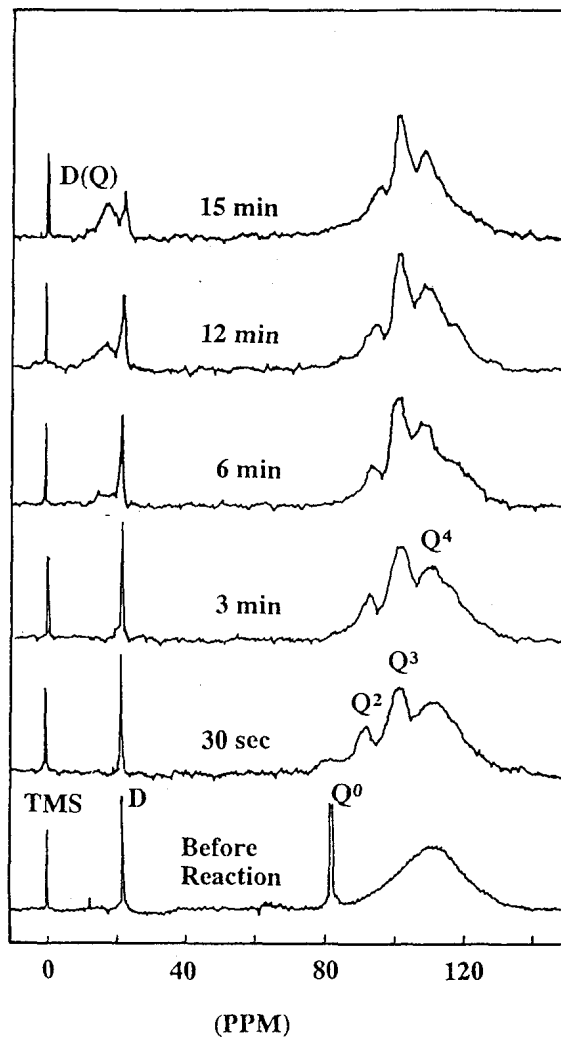


Figure 10. Schematic representation of the structure of the ORMOSIL.

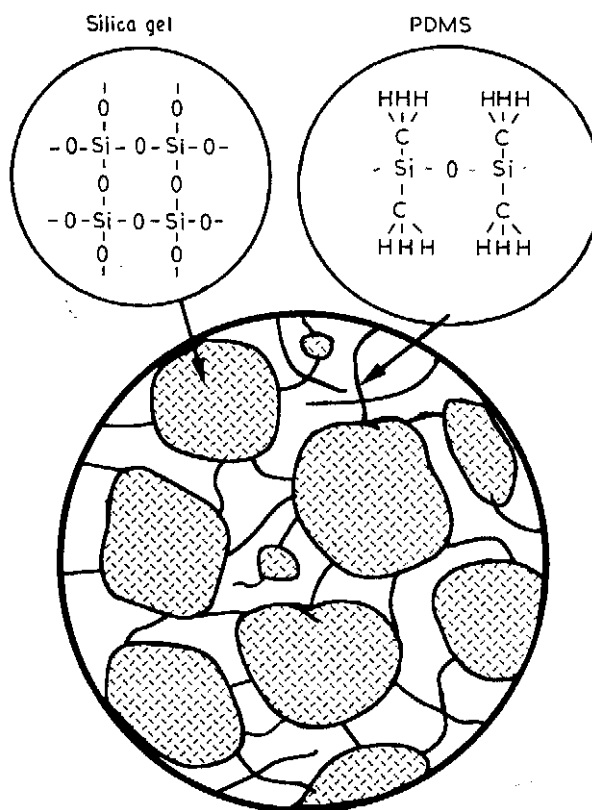


Figure 11. Effect of ultrasonic treatment on the bulk density of gels prepared with various PDMS content.

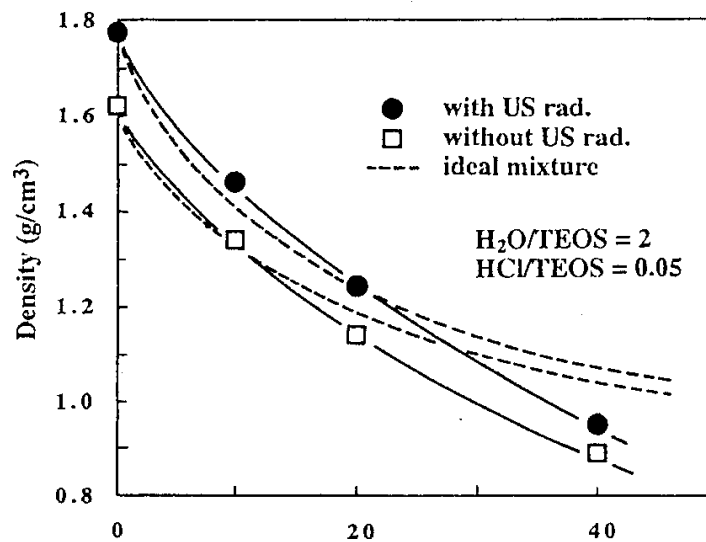


Figure 12. Evolution with time of the relative concentration Q^n silica species deduced from ^{29}Si NMR spectra. C, classic sol; S, sonosol.

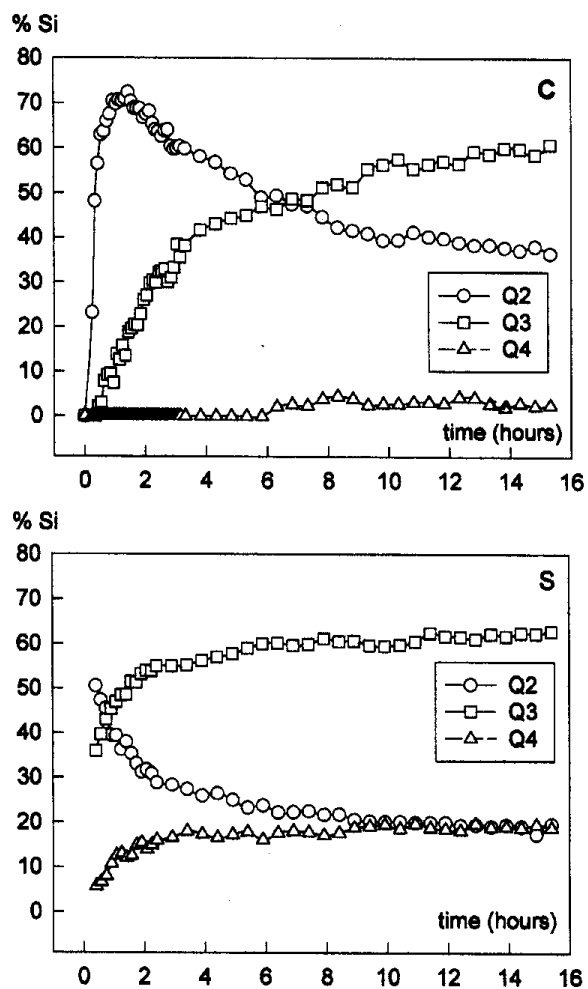


Figure 13. Evolution of the elasticity modulus E' as a function of time for sonogels at different ultrasonic energy doses (U_s in $\text{J}\cdot\text{cm}^{-3}$) and various Water/TEOS molar ratio, n .

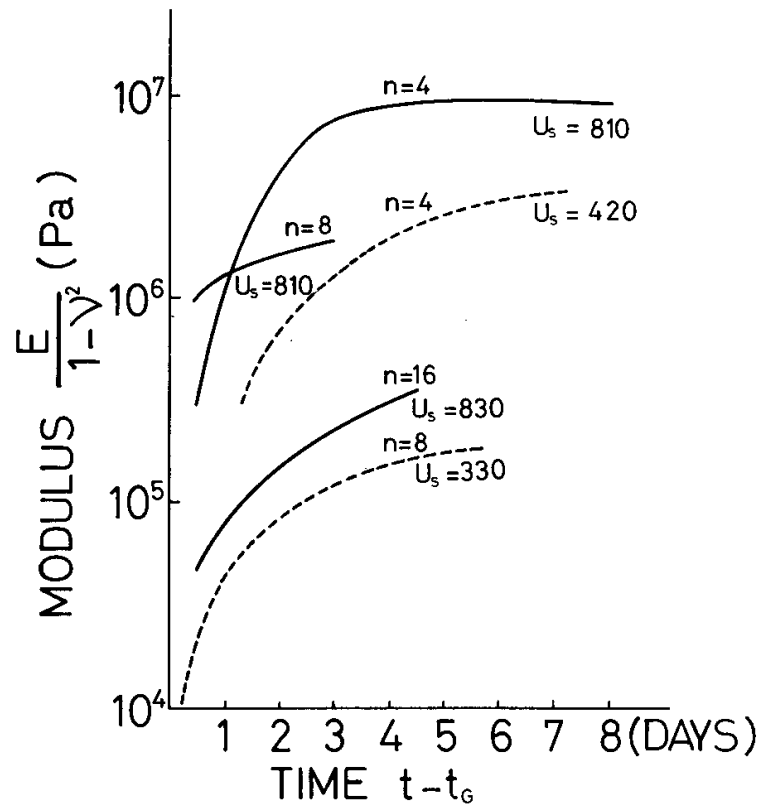


Figure 14. ^{29}Si NMR spectra of 10wt%PDMS-90wt%TEOS solution for several ultrasonic energy doses ($U_s=76 \text{ t (J}\cdot\text{cm}^{-3})$ time in min).

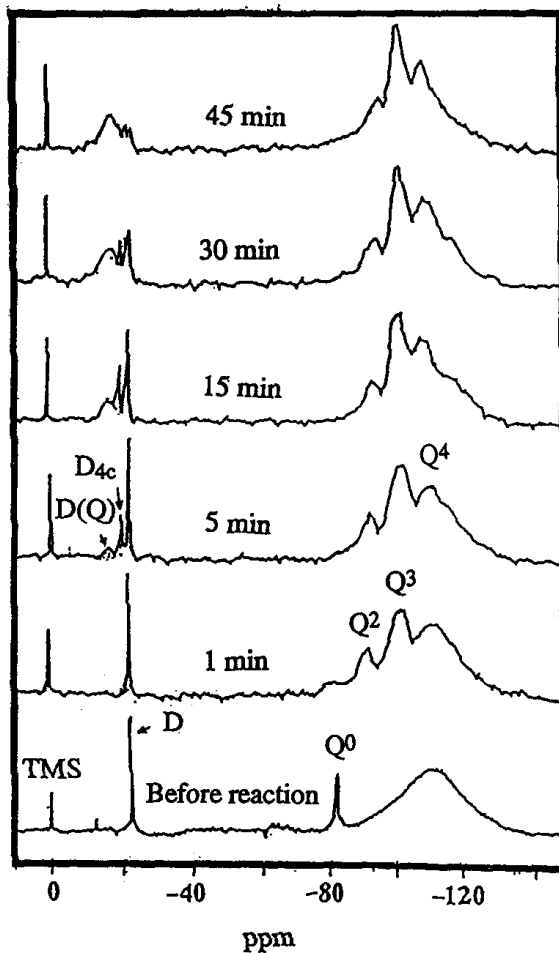


Figure 15. RDFs of sono and classic aerogels. Silica glass RDF is also included for comparison. Arrow in sonogel indicates the break point of the structure.

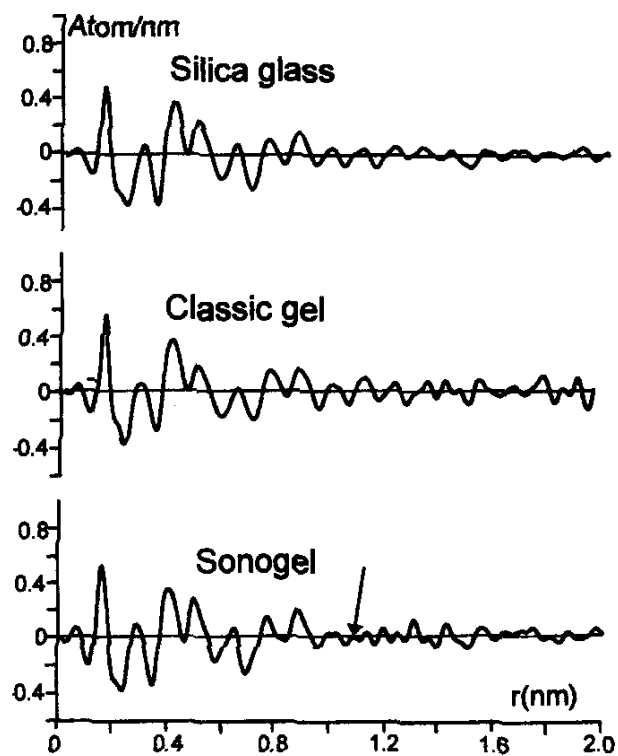


Figure 16. ^{29}Si MAS NMR spectra of (a) sono Sn and (b) classic Cn aerogels prepared with different amount of water/TEOS molar ratio, n .

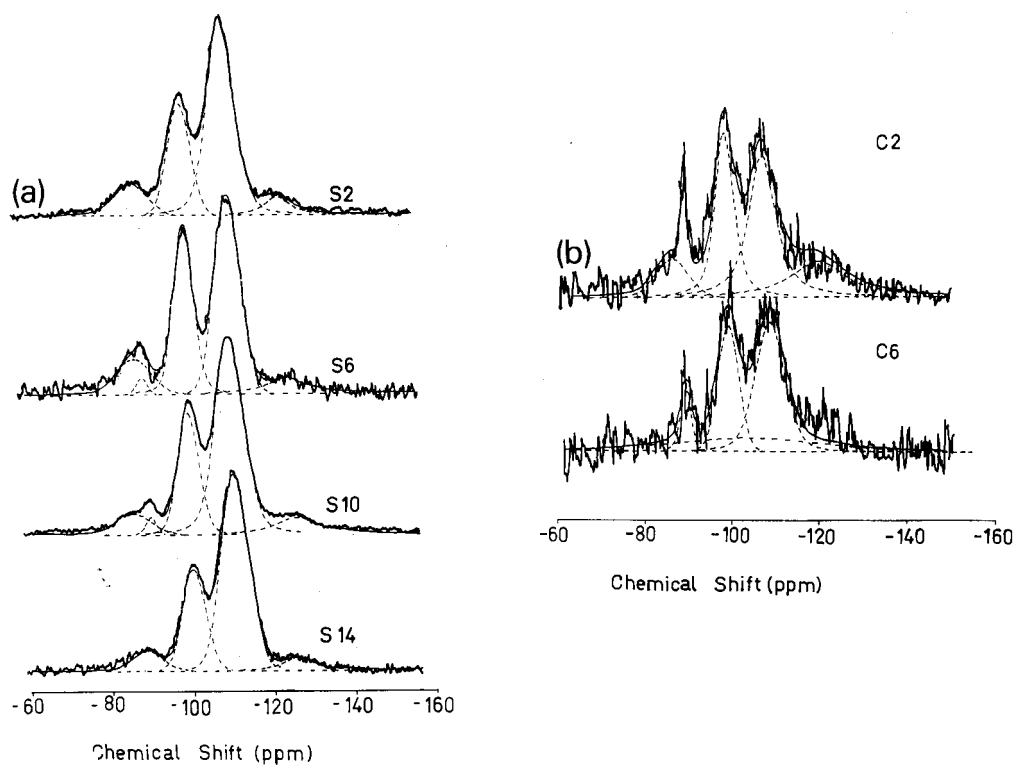


Figure 17. TGA yield for PDMS/TEOS aerogels in air and nitrogen atmosphere.

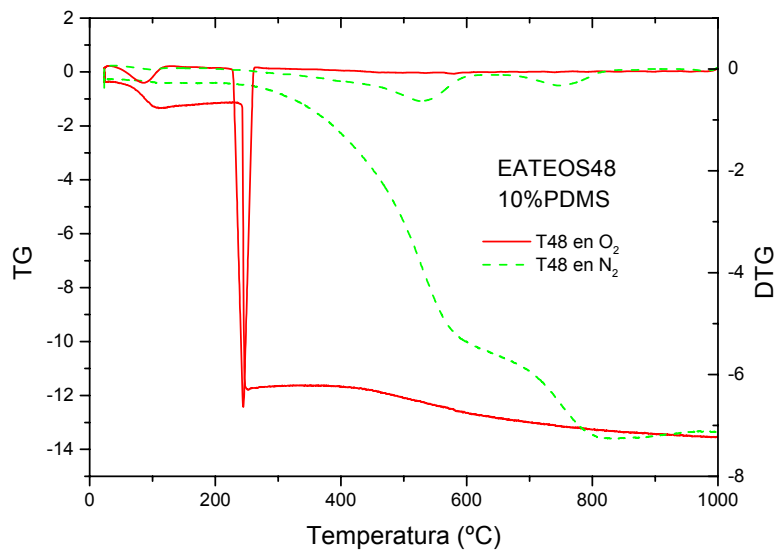


Figure 18. Rubbery ormosils under compressing

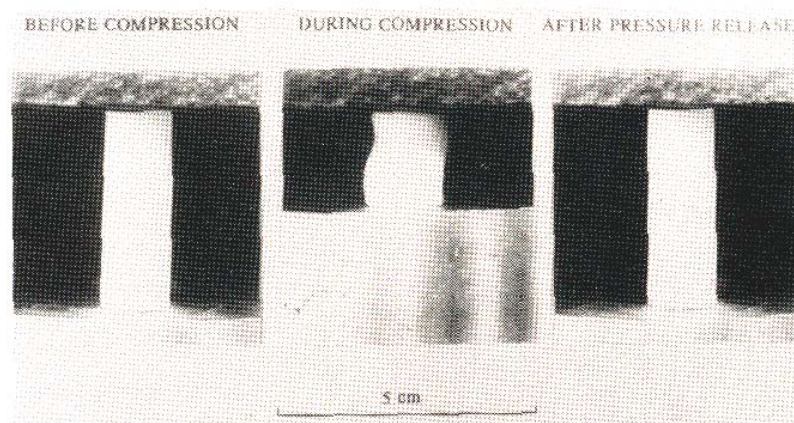


Figure 19 (a) Model 1 with all silica gel species separated by PDMS (b) Model 2 with all silica gel species connected (c) Model 3, a structure between Model 1 and Model 2.

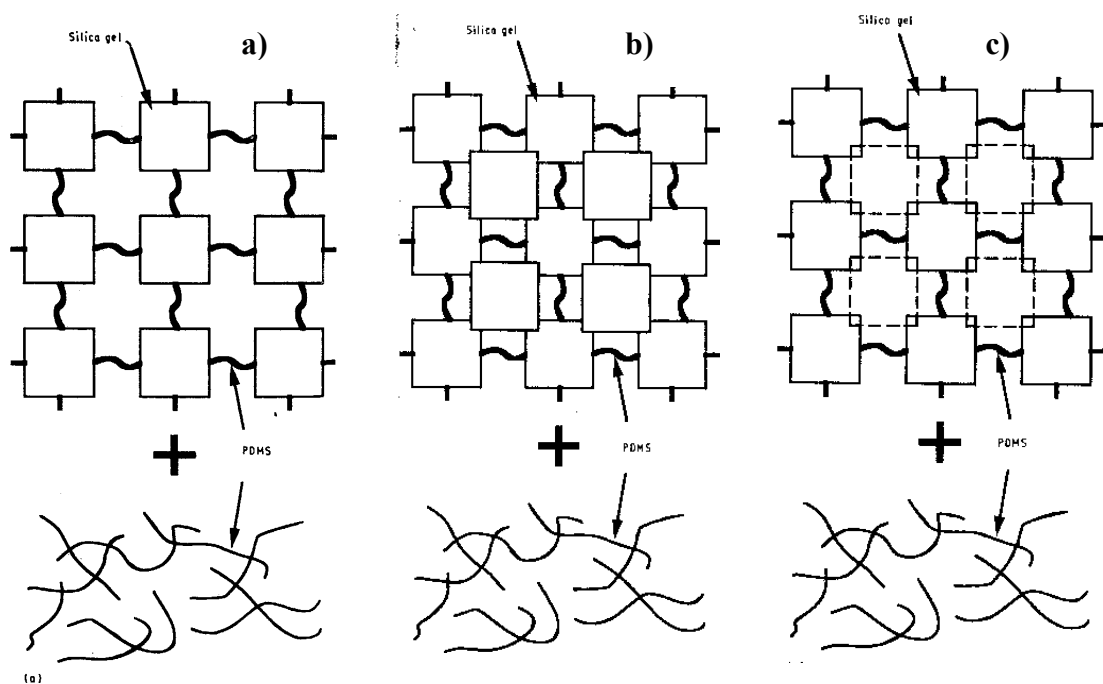


Figure 20. Fracture surface of the sample with the composition TEOS/PDMS = 80/20.



Figure 21. Effect of reaction time on gel microstructure. $[HCl]/[TEOS] = 0.2$. Reaction time: only variable, (A) 30 min, (B) 40 min, (C) 50 min, (D) 60 min.

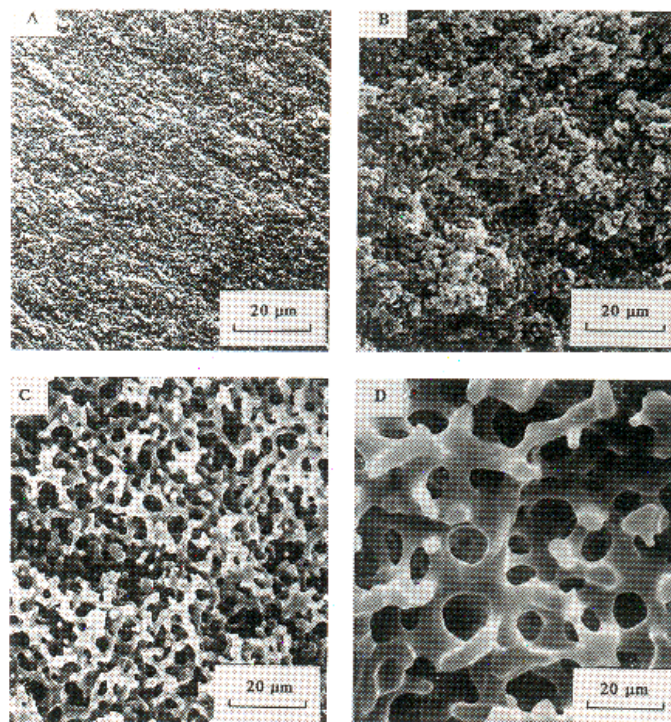


Figure 22. . Evolution of elastic modulus of ORMOSILs versus the PDMS content and for various PDMS molecular weights. (O Foussaier)

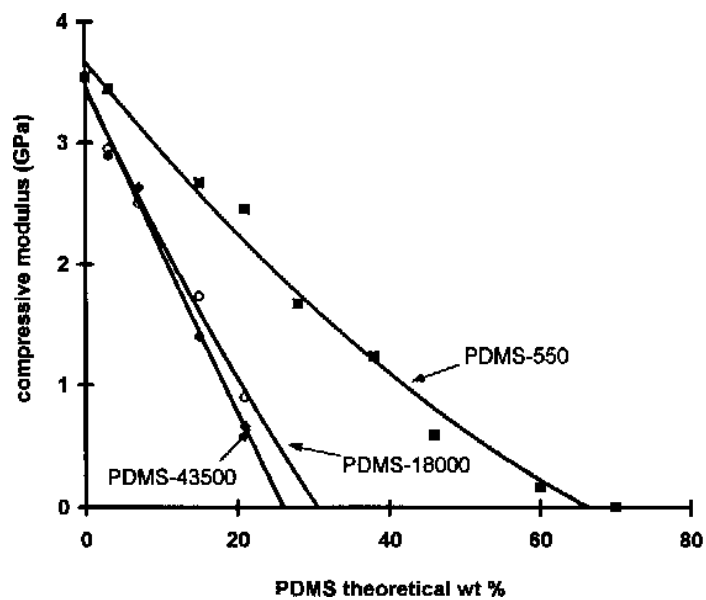


Figure 24.(a) Elastic moduli and (b) Vickers hardnesses of the TEOS/PDMS system hard ormosils.

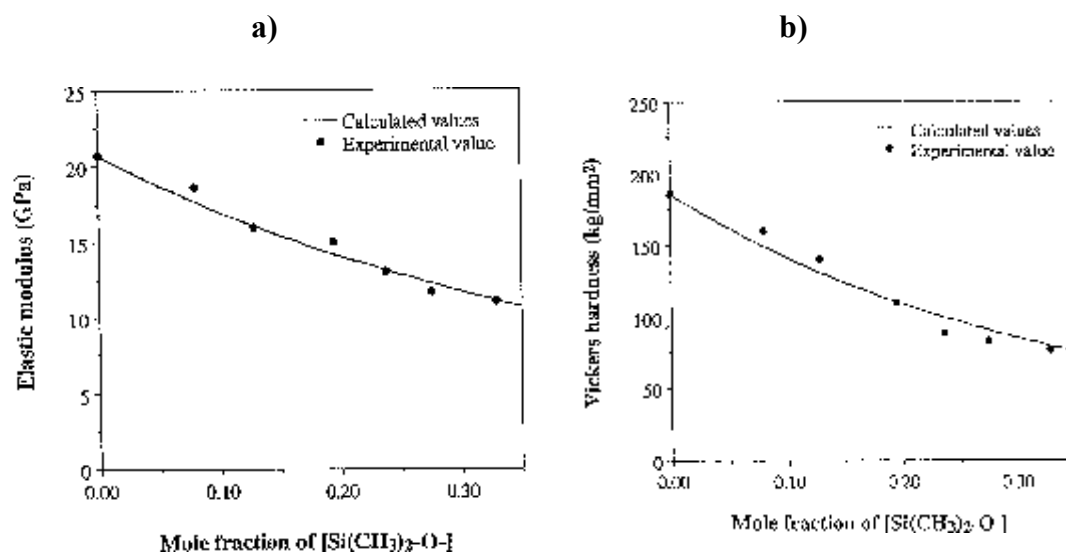


Figure 25. Comparison of the optical gain of Rh610 hosted in (●)PT-Ormosil and (○) PMMA as a function of the number of laser pulses.

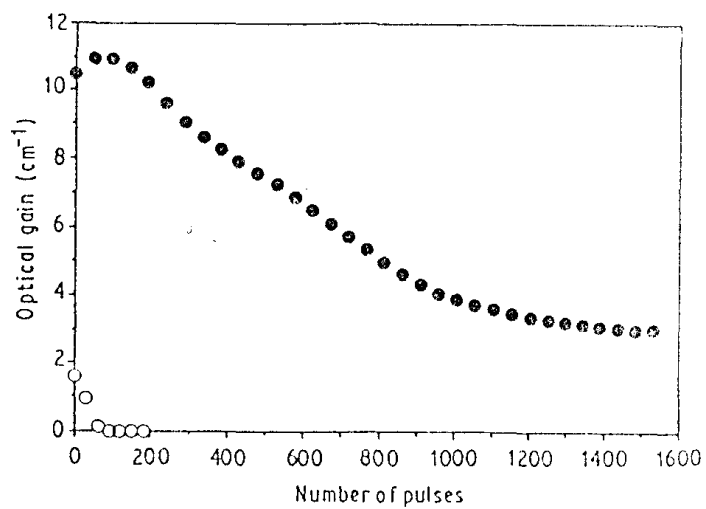


Figure 26. Refraction index of the PhTES/TEOS films prepared from sols hydrolysed with two different acid concentrations, before drying, as a function of PhTES content in the starting solution. Data from [131] is included for comparison.

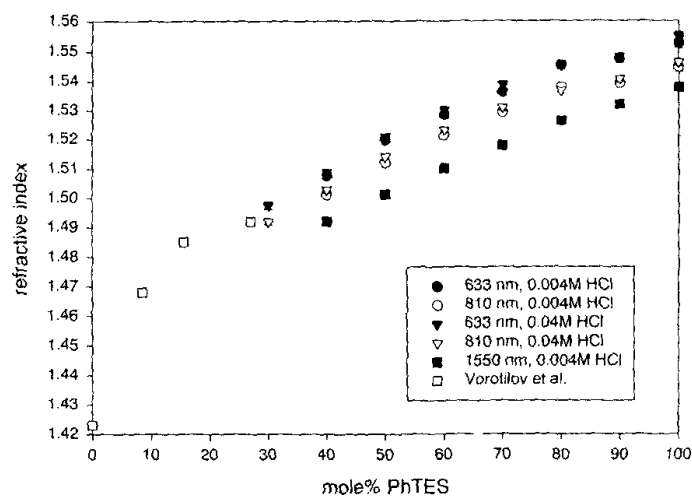


Figure 27. Refractive index of MTES/PhTES/TEOS (a) $x / (80-x) / 20$ films (b) $x / (70-x) / 30$ films prepared from sols hydrolysed with two different acid concentrations, before drying, as a function of PhTES content in the starting solution

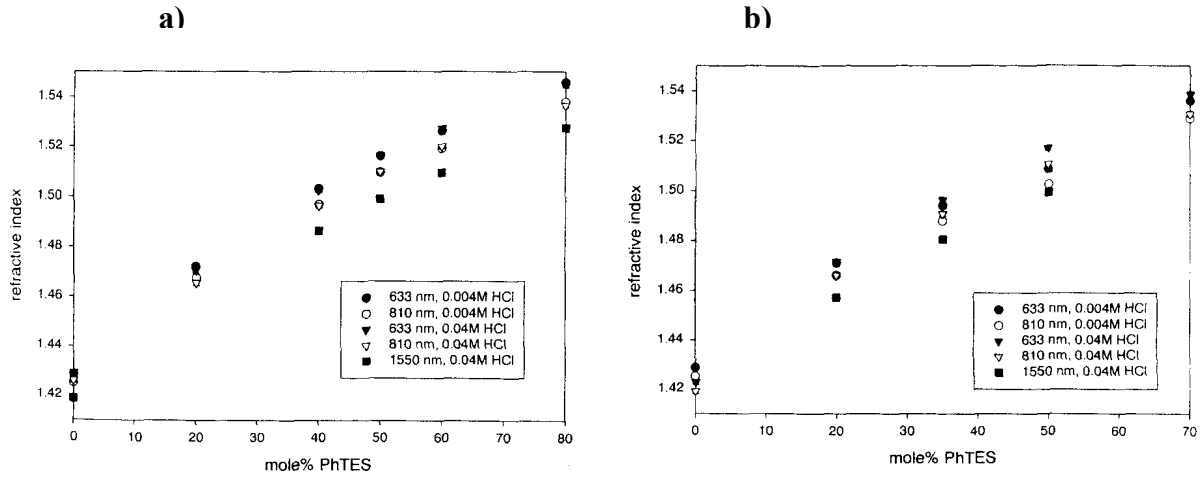


Figure 28. Intensity profile of a gaussian laser beam 0.6 m after passage through a CuPc-sonogel composite (5×10^{-5} M CuPc concentration) Incident intensity on the sample was $I = 2.0 \times 10^5 \text{ W m}^{-2}$

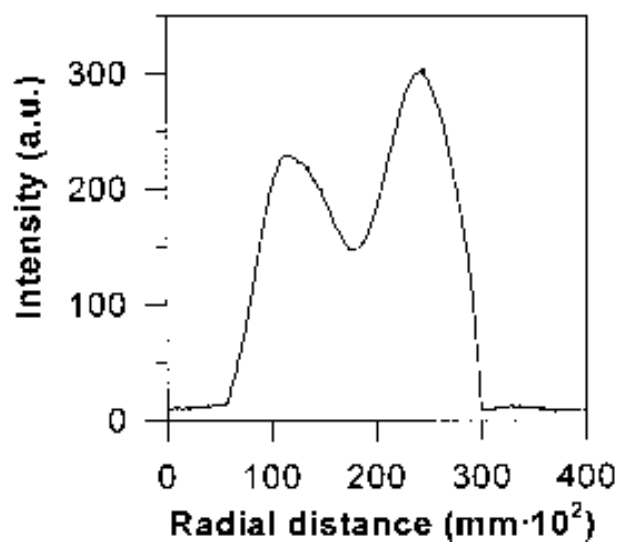


Figure 29. Schematic experimental route for preparing PbS-SiO₂ composites by the sonocatalytic method.

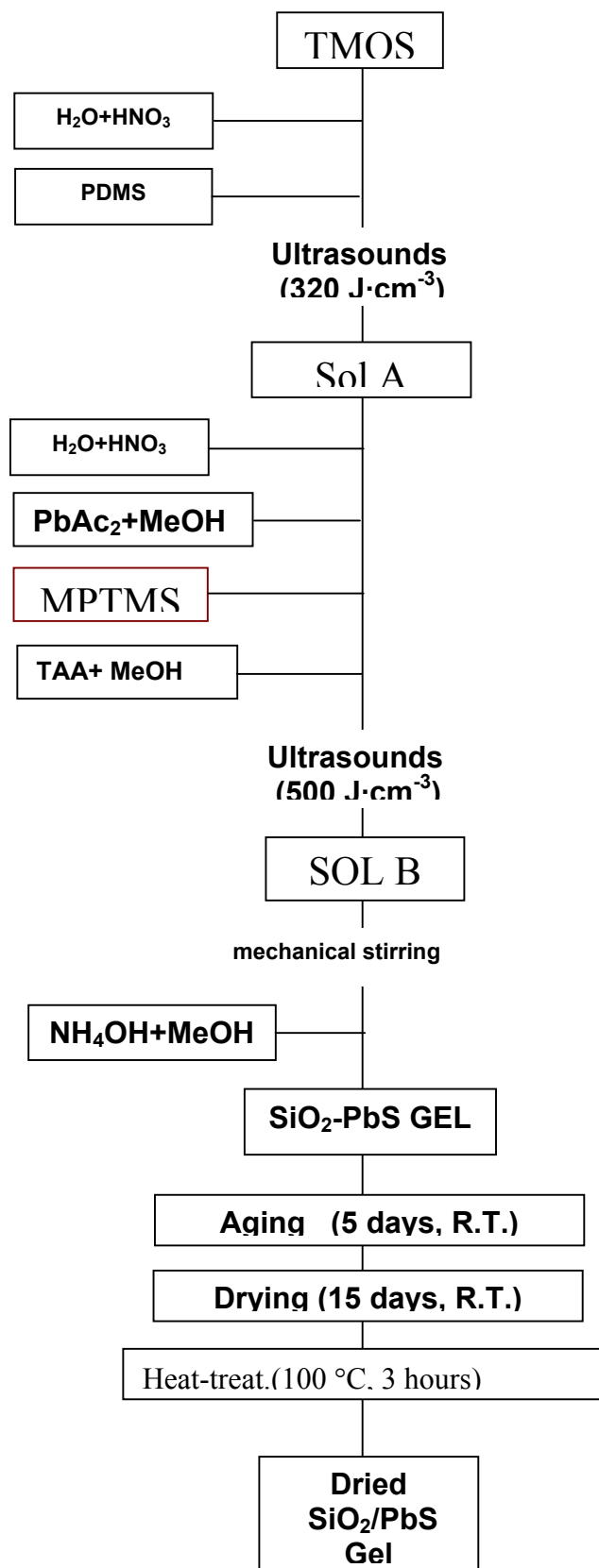


Figure 30. N₂ physisorption isotherms of the 0.5R32, undoped matrix and 4R5 samples. Solid and open symbols correspond to the adsorption and desorption branch, respectively.

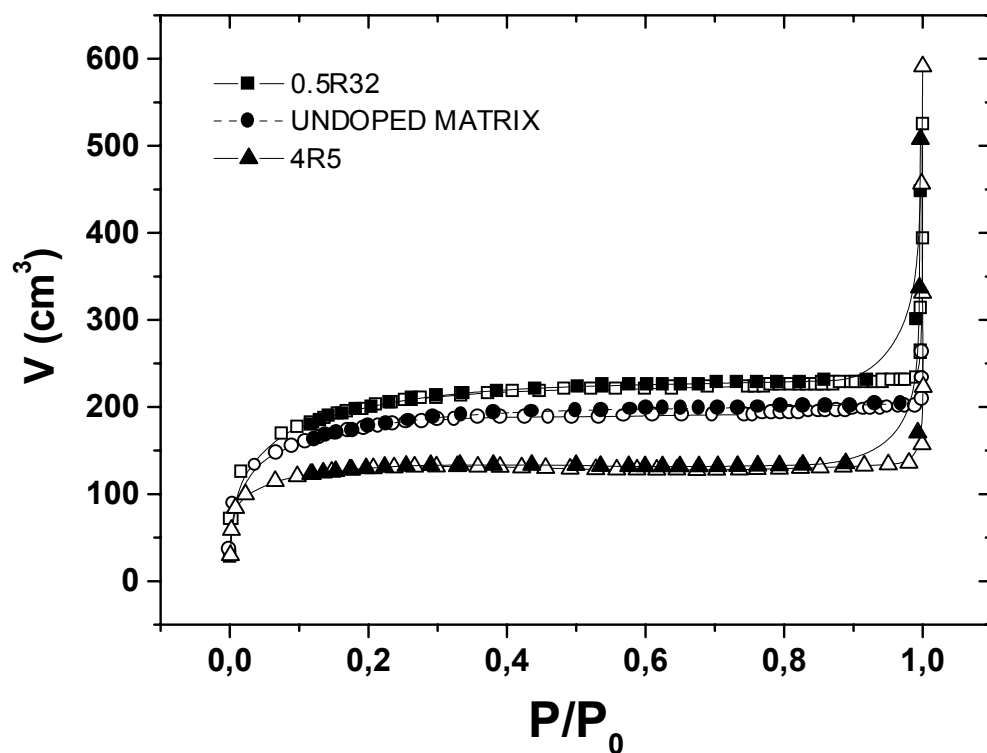


Figure 31. (a)HRTEM micrograph of PbS nanoparticles of the 0.5R32 sample. (b) particle size diameter distribution and, in the inset, the electron diffraction pattern with the corresponding values of interplanar spacing.



Figure 32. Optical absorption spectra of 0.5R32, 1R10 and 4R5 samples. The undoped matrix absorption curve has been also included to notice its transparency in all spectral range where samples behave its bandgap

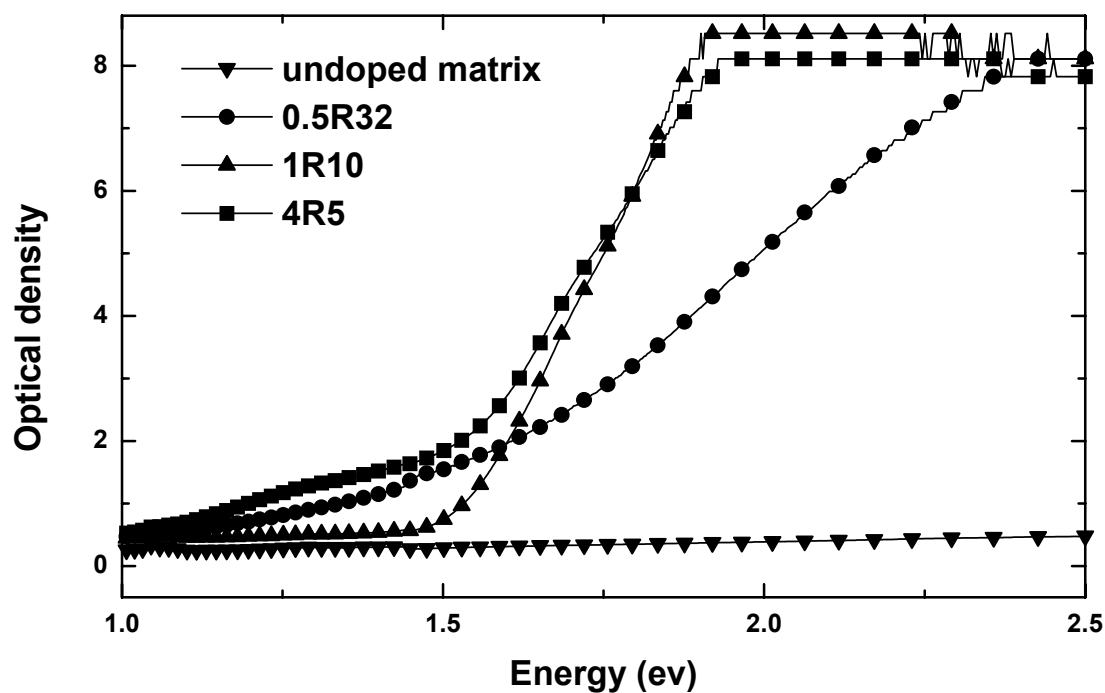
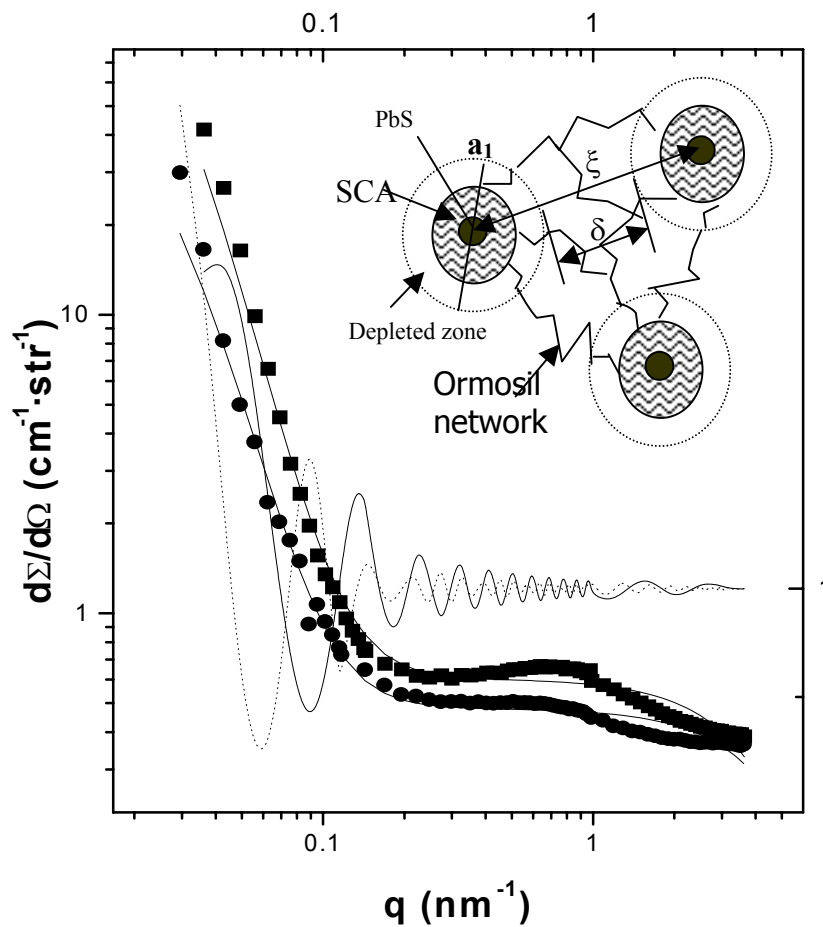


Figure 33. Decovolution of the experimental (dotted line) SANS patterns of PbSEDTA1(■) and 1R10 (●) samples, calculated by using a scattering factor from a two-correlation function combined with Percus-Yevick hard-spheres model. The divergence of the fit (continuous line) at high-q is due to the incoherent scattering contribution from H in the polymer chains. The structure factor from both the PbSEDTA1 sample (continuous line) and the 1R10 one (dotted line) are also depicted and exhibit oscillation around unity. Inset shows the proposed structure model for PbS doped sono-ormosil



REFERENCES

- 1 J.J. Ebelmen, *C. R. Acad. Sci.* **19**, 398 (1844).
- 2 Dislich, H, *Angewandte Chemie*, International Edition, 1971,10, (6): 363.
- 3 Roy, R, *J. Am. Ceram. Soc.* 1969, 52 : 344.
- 4 H. Schroeder, *Phys. Thin Films* 5, 87 (1967).
- 5 D. R. Secrist, and J. Mackenzie D, *Modern Aspect Vitreous State*, 1964, 3: 149.
- 6 Hench, L L and J. K. West, *Chem. Rev.* 1990, 90 : 33.
- 7 Ulrich D R, *J. Non-Cryst. Solids* 1988, 100 : 174.
- 8 Mackenzie, J D, *J. Non-Cryst. Solids* 1982, 41 : 1.
- 9 Sakka, S, Kamiya, KJ, *J. Non-Cryst. Solids* 1980, 42 : 403.
- 10 Dislich, H, *J. Non-Cryst. Solids* 1985, 73 : 599.
- 11 Yamane, M, Aso, S, Sakaino, T, *J. Mater. Sci.* 1978, 13 : 865.
- 12 J. Brinker and G. Scherer, "Sol-Gel Science: the physics and chemistry of sol-gel processing". Academic Press, San Diego, CA. 1990.
- 13 Davis, J T, Rideal, E K, *Interfacial Phenomena*, Academic Press, New York, 1963.
- 14 Flory, P J, *Faraday Disc. Chem. Soc.*, 57, 1974: 7
- 15 Rabinovich, E M, in *Sol-gel Technology for Thin Films, Fibers, Preforms, Electronics and Special Shapes*, Klein, L C, ed. (Noyes, Park Ridge, N.J., 1988), pp. 260-294.
- 16 Philipp G and Schmidt H, *J. Non-Cryst. Solids*, 1984, 63: 283.
- 17 Wilkes G, Orler B, and Huang H, *Polym. Prep.* , 1985, 26 (2): 47.
- 18 Huang H, Orler B, and Wilkes G L, *Polymer Bull.* , 1985, 14: 557.
- 19 Schmidt H, *J. of Non-Cryst. Solids*, 1985, 73: 681.
- 20 *Better Ceramics Through Chemistry VII: Organic/Inorganic Hybrid Materials* B.K. Coltrain, Sánchez C, Schaefer D W and Wilkes G L, (eds) MRS Symp. Proc. Vol. 435, 1996.
- 21 *Organic/Inorganic Hybrid Materials*, Klein L and Sánchez C (eds) *J.Sol-Gel Sci.&Tech.*, 5 (2), 1995 and 7 (3), 1996, (special issues).
- 22 Mackenzie J D, *J. of Sol-Gel Science&Technology*, 2, 81 (1994).
- 23 P. Calvert and S. Mann, *J. Mat. Sci.* 23, 3801 (1988).
- 24 R.Z. Wang, Z. Suo, A.G. Evans, N. Yao and I.A. Aksay, *J. Mater. Res.* 16, 2485 (2001)
- 25 H. Schmidt, *J. Non-Cryst. Solids* 112, 419 (1989).
- 26 Chemistry of Materials, "Organic-Inorganic Nanocomposite Materials" Vol. 13, 3059-3910 (2001)
- 27 C. Sanchez and B. Lebeau, *MRS Bulletin* (May 2001) p. 377.
- 28 C. Sanchez and F. Ribot, *New J. Chem.* 18, 1007 (1994)
- 29 D. Avnir, D. Levy and R. Reisfeld, *J. Phys. Chem.* 88, 5956 (1984)
- 30 A. Makishima and T. Tani, *J. Am. Ceram. Soc.* 69, C-72 (1986)
- 31 E. Toussaere, J. Zyss, P. Griesmar and C. Sanchez, *Nonlinear Optics* 1, 349 (1991)
- 32 P.N. Prasad, *SPIE Proc.* 1328, 168 (1990)
- 33 R. Zusman, C. Rottman, M. Ottolenghi and D. Avnir, *J. Non-Cryst. Solids* 122, 107 (1990)
- 34 D. Levy, S. Einhorn and D. Avnir, *J. Non-Cryst. Solids* 113, 137 (1989)
- 35 S. Yano, K. Iwata and K. Kurita, *Mater. Sci. And Eng.* C6, 75 (1998)
- 36 Morita K, Hu Y and Mackenzie J D, in *Mat. Res. Soc. Symp. Proc.*, Vol 271, (MRS Ed., 1992) p.693
- 37 Morita K, Hu Y and Mackenzie J D, *J. Sol-Gel Sci. &Tech.*, 3, 109 (1994)

-
- 38 E. Blanco, L. Esquivias, R. Litran, M. Piñero, M. Ramírez-del-Solar and N. de la Rosa-Fox, *Appl. Organomet. Chem.* 13, 399 (1999)
- 39 J.D. Mackenzie, *J. Ceram. Soc. Japan* 101, 1 (1993)
- 40 R. Erce-Montilla, M. Piñero, N. de la Rosa-Fox, A. Santos and L. Esquivias, *J. Mater. Res.* 16, 2572 (2001)
- 41 B. Dunn, J.D. Mackenzie, J.I. Zink and O.M. Stafsudd, *SPIE Proc.* 1328, 174 (1990)
- 42 R.K. Iler, in "The Chemistry of Silica", Wiley, New York, 1979
- 43 M.D. Saks and R-S. Sheu, in "Science of Ceramic Chemical Processing" eds. L.L. Hench and D.R. Ulrich (Wiley, NY, 1986) p. 100
- 44 A.J. Vega and G. Scherer, *J. Non-Cryst. Solids* 111, 153 (1989)
- 45 P.J. Flory, in "Principles of Polymers Chemistry" (Cornell University Press, NY, 1953) Ch. IX
- 46 B. Mandelbrot, in "The Fractal Geometry of the Nature" (Freeman, NY, 1982)
- 47 R. Zallen, in "The Physics of Amorphous Solids" (Wiley, NY, 1983) Ch. 4
- 48 B.H. Zimm and W.H. Stockmayer, *J. Chem. Phys.* 17,1301 (1949)
- 49 J. Zarzycki, in "Science of ceramic chemical processing". L. Hench L and D.R. Ulrich (Ed.) (Wiley, NY, 1986) p. 21
- 50 F.A.L. Dullien, in "Fluid Transport and Pore Structure". (Academic Press, NY, 1979)
- 51 J. Brinker and G. Scherer, *J. Non-Cryst. Solids* 70, 301 (1985)
- 52 J. Zarzycki, M. Prassas and J. Phalippou, *J. Mater. Sci.* 17, 3371 (1982).
- 53 Hench, L L, in *Science of ceramic chemical processing*. L. Hench L and D.R. Ulrich (Ed.) Wiley, New York, 1986, p. 52
- 54 Ramírez-del-Solar M, Esquivias L, Craievich A F, and Zarzycki J, *J. Non-Cryst. Solids*, 1992,147-148: 206.
- 55 Zarzycki J, in *Chemical Processing of Advanced Materials* L. Hench L and J.K. West (Eds.), John Wiley & Sons, Inc., New York, 1992, p. 84.
- 56 Zarzycki J, *J. Non-Cryst. Solids*, 1992, 147&148: 176.
- 57 Rodríguez Ortega J, *Ph. D. Thesis*. University of Cádiz. Cadix. Spain (1996).
- 58 Rodríguez-Ortega J and Esquivias L, *J. Sol-Gel Sci. Tech.* 1997 8: 117.
- 59 Blanco E, de la Rosa-Fox N, Esquivias L, and Craievich A F, *J. Non-Cryst. Solids*, 1992, 147-148: 296.
- 60 Kistler S S, *J. Phys.Chem.*, 1932, 36: 52.
- 61 Nicolaon G A and Teichner S J, *Bull. Soc. Chim. Fr.* , 1968: 1900
- 62 Prassas M, *Ph. D. Thesis*. University of Montpellier II, Montpellier, France (1981)
- 63 Zarzycki J, Prassas M and Phalippou J, *J. Mater. Sci.*, 1982, 17: 3371
- 64 Prassas M, Phalippou J and Zarzycki J, *J. Phys C-9*, 1982, 43: 257
- 65 Phalippou J, Woignier T and Zarzycki J in *Ultrastructure Processing of Ceramics, Glasses and Composites* D.R. Uhlmann and D.R. Ulrich (Eds) Wiley Interscience, N.Y., 1984, pp 70-87
- 66 Woignier T, *Ph. D. Thesis*, University of Montpellier II, Montpellier, France (1984)
- 67 *Aerogels*. Proceeding of the 1st International Symposium on Aerogels (ISA1), Fricke J, Ed. Springer-Verlag, Berlin, (1986).
- Proceedings of ISA2, *J. de Physique Appliquée*. Supplément au n° 4. C4-1989., Vacher R, Phalippou J., Pelous J, Woignier T, Eds. (1989).
- Proceedings of ISA3, *J. Non-Cryst. Solids*,. 145. (1992) Fricke J., Ed.
- Proceedings of ISA 4, *J. Non-Cryst. Solids*, 186 (1995). Pekal R W, Hrubesch L W, Eds)

-
- Proceedings of ISA 5, *J. Non-Cryst. Solids*, , 225 (1997). J. Phalippou and R Vacher, Eds
- 68 Zarzycki J, *J. Non-Cryst. Solids*, 1990, 121:
- 69 Fricke J ed., *Aerogels*, Springer Proceeding in Physics, Vol 6, Springer, Heidelberg, 1986.
- 70 Fricke J and Emmerling A, in *Aerogels- Preparation, Properties, Applications* R. Resifeld and C.K. Jørgensen (Ed.), Springer Series Structure and Bonding. Vol. 177, Springer, Heidelberg, 1992, p. 37.
- 71 Fricke J, *J. Non-Cryst. Solids*, 1992,147-148:356
- 72 M. Prassas, J. Phalippou and J. Zarzycki in "Science of Ceramic Chemical Processing" eds. L.L. Hench and D.R. Ulrich (Wiley, NY, 1986) p. 156.
- 73 H. Zang and C. Pantano, *J. Am. Ceram. Soc.* 73, 958 (1990).
- 74 F. Babonneau, L. Bois and J. Livage, *J. Non-Cryst. Solids* 147&148, 280 (1992)
- 75 J. Zarzycki, *Heterogeneous Chemistry Reviews*, , 1, 243 (1994)
- 76 Lorimer J P and Mason T J , *Chem. Soc. Rev.*, ,16, 239 (1987)
- 77 Neppiras E A, *Ultrasonics*, 22-1 , 25 (1984)
- 78 G.J. Price, *Ultrasonics Sonochem.* 3, 5229 (1996)
- 79 J.L. Luche, in "Current Trends in Sonochemistry" Ed. G.J. Price (RSC, Cambridge, 1992) p. 34
- 80 T.J. Mason, in "Practical Sonchemistry" (Ellis Horwood, Chichester, 1991)
- 81 P. Kruus, *Ultrasonics* 21, 201 (1983)
- 82 P. Boudjouk, in "Science of Ceramics Chemical Processing" eds. L.L. Hench and D.R. Ulrich (Wiley, NY, 1986) p. 363
- 83 G.J. Price, M.P. Hearn, E. Wallace and A.M. Patel, *Polymer* 37, 2303 (1996)
- 84 Tarasevich M, *Cer. Bull.*, 63, 500 (Abstract only) (1984)
- 85 Esquivias L and Zarzycki J, in *Current Topics on Non Crystalline Solids*, Baró M D and Clavaguera N(Eds.), (World Scientific, Singapore, 1986), p. 409
- 86 Esquivias L and Zarzycki J, in *Ultrastructure Processing of Ceramics, Glasses and Composites*. Mackenzie J D and D.R. Ulrich, (Eds.) (Wiley, NY, 1988) p. 255.
- 87 de la Rosa-Fox N, Esquivias L and Zarzycki J, *Diffusion and Defect Data*, 53-54, 363 (1987)
- 88 E. Blanco, Ph. D. Thesis. Universidad de Cádiz. 1993
- 89 Hummel D, Torriani I L, Ramos A Y , Craievich A F, de la Rosa-Fox N, Esquivias L in "Better Ceramics Through Chemistry V",: C. Ed. Sanchez C, (Material Research Society Press Pittsburgh EE.UU, 1994) p. 673
- 90 Litrán R, Petersen P M, Johansen P M, Linvold L, Ramírez-del-Solar M and Blanco E, *J. of Appl. Phys.*, 81, 7728 (1997)
- 91 Petersen P M, Litrán R, Johansen P M and L. Lindvold, in *SPIE Proc.* 2788: 202 (1996)
- 92 García-Hernández M, Jiménez-Riobóo R , Prieto C , Fuentes-Gallego J J, Blanco E and Ramírez-del-Solar M, *Appl. Phys. Lett.* , 69, 3827(1996)
- 93 Jiménez-Riobóo R , García-Hernández M, Prieto C , J.J. Fuentes-Gallego, Blanco E and M. Ramírez del Solar, *J. Appl. Phys.*, 81, 7739 (1997).
- 94 H-J. Tiller, R. Gobel and U. Hartung, *J. Non-Cryst. Solids* 105, 162 (1988)
- 95 H. Coudurier, R. Baudru and J.B. Donnet, *Bull. Soc. Chim. Fr.* 9, 3147, 3154 and 3161 (1971)
- 96 Mackenzie J.D., Chung Y.J. and Hu Y., *J. Non-Cryst. Solids* 147&148, 271 (1992).
- 97 O. Foussaier, M.Menetrier, J.-J. Videau, E. Duguet, *Mat Lett.* 42, 305 (2000)
- 98 G-D. Kim, D-A. Lee, J-W. Moon, J-D. Kim and J-A. Park, *Appl. Organomet. Chem.* 13, 361 (1999)
- 99 E. Geissler, F. Horkay, A-M. Hecht, C. Rochas, P. Lindner, C. Bourgaux and G. Couarraze, *Polymer* 38, 15 (1997)
- 100 P. Debye and A.M. Bueche, *J. Chem. Phys.* 16, 573 (1948)

-
- 101 P. Lindner, in "Modern Aspects of Small-Angle Scattering" Ed. H. Brumberger (Kluwer, Dordrecht, 1993) p. 409. A.R. Rennie in p. 433.
- 102 T. Iwamoto, K. Morita and J.D. Mackenzie, *J. Non-Cryst. Solids* 159, 65 (1993).
- 103 H. Marsmann, in "NMR, Oxygen-17 and Silico-29" eds. P. Diehl, E. Fluck and R. Kosfeld (Springer, Berlin, 1981) p. 65
- 104 Blanco E, García-Hernández M, Jiménez-Riobóo R, Litrán L, Prieto C and Ramírez-del-Solar M, *J. Sol-Gel Sci. And Tech.* 13, 451 (1998).
- 105 Pérez-Moreno A, Jiménez-Solís C, Esquivias L and de la Rosa-Fox N, presented at the Bienal de la Sociedad Española de Cerámica y Vidrio, San Sebastián (Spain) 1996
- 106 de la Rosa-Fox N, Esquivias L and Zarzycki J, *J. Mater. Sci. Lett.*, 10, 1237 (1991)
- 107 J. Zarzycki, *J. Non-Cryst. Solids* 100, 359 (1988)
- 108 T. Iwamoto and J.D. Mackenzie, *J. of Sol-Gel Science&Technology*, 4, 141 (1995).
- 109 Wei W, *J. Non-Cryst. Solids*, **81**, (1986) 239.
- 110 Rosenthal A B and Garofalini S, *J. Non-Cryst Solids* **107**, (1988) 65
- 111 Warren B E, in "X-ray Diffraction", Adisson-Wesley, New York, (1969)
- 112 Barrera-Solano C, de la Rosa-Fox N and Esquivias L, *J. Non-Cryst. Solids*, , 147&148, 194 (1992)
113. Y. Sorek, R. Reisfeld, I. Finkelstein, S. Ruschin, *Appl.Phys.Lett.* 63 (1993) 3256.
114. D.-K Qing, K. Itoh., M. Murabayashi, *Chem.Lett.* (1996) 623.
115. K. A. Vorotilov, V.A.Vasilijev, M.V. Sobolevsky, N.I. Afanasyeva, *Thin Solid Films* 288 (1996) 57.
116. K.-H. Haas, S. Amberg-Schawb, K. Rose, G. Schottner, *Surf. Coat. Technol.* 111 (1999) 72.
117. Y. Hu, J. D Mackenzie, *J. Mat Sci.* 27 (1992) 4415
118. Y. Hu and J. D. Mackenzie, *Mat. Res. Soc. Symp. Proc. Vol. 271* (1992) 681
119. W. Que, S. Sun, Y. Zhou, Y.L. Lam, S.D. Cheng, Y.C. Chan, C.H. Kam, *Mat Lett.* 42 (2000) 326.
120. T. Iwamoto, J. Mackenzie, *Mat. Res. Symp. Proc. Vol 346 MRS* (1994) 397
121. A. Makishima, J.D. Mackenzie, *J. Non-Cryst. Solids* 17 (1975) 147.
122. A. Makishima, J.D.Mackenzie, *J. Non-Cryst. Solids*, 12 (1973) 35.
123. M. Yamane, J. D. Mackenzie, *J. Non-Cryst. Solids*, 15 (1974) 153.
124. B. A. Auld, in *Acosutic Fields and Waves in Solids* (Wiley, New York, 1973)
125. H.-T. Lin, E. Bescher, J.D. Mackenzie, H. Dai, O.M. Stafsudd. *J. Mat Sci.* 27 (1992) 5523.
126. F. Gan. *J. Sol-Gel Sci.Tech.* 13 (1998) 559
127. T. Takada, T. Yano, A. Yasumori, *J. Non-Cryst. Solids* 147&148, (1992) 631.
128. P. Innocenzi, A. Martucci, M. Guglielmi, L. Armelao, S. Pelli, G.C. Righini, G.C. Battaglin, *J. Non-Cryst. Solids* 259 (1999) 182
129. K. Tadanaga, B. Ellis, A. Seddon, *J. Sol-Gel Sci.Tech.* 19 (2000) 687
130. G.R. Atkins, R. M. Krolikowska, A. Samoc, *J. Non Cryst. Solids* 265 (2000) 210.
- 131 K.A. Vorotilov, V. I. Petrovsky, V.A.Vasiljev, M.V. Sobolevsky, *J-Sol-Gel Sci. Tech.* 8. 581 (1997)
132. D. Levy, D. Avnir, *J. Phys. Chem.* 92 (1998) 4734.
133. M. Canva, P.Georges, A. Brun, D. Larrue, J. Zarzycki, *J. Non- Cryst. Solids* 147&148 (1992) 627
134. R. Litrán, E. Blanco, M. Ramírez-del-Solar, N. De la Rosa-Fox, L. Esquivias, *J. Sol-Gel Sci. Tech.* 8 (1-3) (1997) 985
135. D. Dolphin (ed) "The Porphyrins", Vols. 1-7 Academic Press, New York (1978)
136. E. Blanco, D. Narayana Rao, F.J. Aranda, D.V.G.L.N. Rao, S. Tripathy, R. Litrán, M. Ramírez-del-Solar, *J. Appl. Phys.* 83 (3) (1998) 634.

-
- 137 M.Piñero, N. De la Rosa-Fox, R. Erce-Montilla, L.Esquivias, J. Sol-Gel Sci. And Tech.
(2002) in press
138. U. Keiderling, Physica B, 1111 (1997) 234